molecules

MDPI

Review

Progress on Noble Metal-Based Catalysts Dedicated to the Selective Catalytic Ammonia Oxidation into Nitrogen and Water Vapor (NH_3-SCO)

Magdalena Jabłońska

Institute of Chemical Technology, Universität Leipzig, Linnéstr. 3, 04103 Leipzig, Germany; magdalena.jablonska@uni-leipzig.de

Abstract: A recent development for selective ammonia oxidation into nitrogen and water vapor (NH_3-SCO) over noble metal-based catalysts is covered in the mini-review. As ammonia (NH_3) can harm human health and the environment, it led to stringent regulations by environmental agencies around the world. With the enforcement of the Euro VI emission standards, in which a limitation for NH_3 emissions is proposed, NH_3 emissions are becoming more and more of a concern. Noble metal-based catalysts (i.e., in the metallic form, noble metals supported on metal oxides or ion-exchanged zeolites, etc.) were rapidly found to possess high catalytic activity for NH_3 oxidation at low temperatures. Thus, a comprehensive discussion of property-activity correlations of the noble-based catalysts, including Pt-, Pd-, Ag- and Au-, Ru-based catalysts is given. Furthermore, due to the relatively narrow operating temperature window of full NH_3 conversion, high selectivity to N_2O and NO_x as well as high costs of noble metal-based catalysts, recent developments are aimed at combining the advantages of noble metals and transition metals. Thus, also a brief overview is provided about the design of the bifunctional catalysts (i.e., as dual-layer catalysts, mixed form (mechanical mixture), hybrid catalysts having dual-layer and mixed catalysts, core-shell structure, etc.). Finally, the general conclusions together with a discussion of promising research directions are provided.

Keywords: noble metals; supported oxides; bifunctional catalysts; NH_3-SCO

check for updates

Citation: Jabłońska, M. Progress on Noble Metal-Based Catalysts Dedicated to the Selective Catalytic Ammonia Oxidation into Nitrogen and Water Vapor (NH_3-SCO). *Molecules* **2021**, *26*, 6461. https://doi.org/10.3390/molecules26216461

Academic Editors: Francesco Enrichi, Alberto Vomiero, Elti Cattaruzza and Piersandro Pallavicini

Received: 21 September 2021
Accepted: 25 October 2021
Published: 26 October 2021

1. Introduction

Ammonia (NH_3) is a corrosive, highly toxic, and reactive inorganic gas with a pungent odor under ambient conditions. It is an atmospheric pollutant that is dangerous to health and life because it could corrode skin, eyes, and lungs, and cause permanent injury or even death when the concentration is higher than 300 ppm [1,2]. Ammonia is also reported to be the most common pollutant found in water streams, further affecting human health as the consequence of eating toxic fish and drinking water [3]. The toxic action of ammonia on aquatic animals can lead to the extinction of the entire population, threatening many important ecosystems and fisheries worldwide [4,5]. NH_3 is referred to as one of four major atmospheric pollutants together with NO_x, SO_x, and nonmethane volatile organic compounds (NMVOC). Approximately 5600 kt y^{-1} of ammonia are emitted into the atmosphere each year, i.e., up to 4-times higher emission levels than in the previous century, and it continues to increase [6]. NH_3 is emitted by several various processes, including nitric acid production, urea manufacturing, nitrogen fertilizer production, biomass, and coal gasification, petroleum refining and refrigeration, livestock waste, and animal agriculture, transport (as a gas slip from the process of selective catalytic reduction of NO_x using NH_3 or urea (SCR) in $DeNO_x$ applications), etc. More attention was given to the removal of NH_3 from gaseous and waste streams, e.g., through its oxidation.

The selective catalytic oxidation of ammonia (NH_3-SCO) into nitrogen and water vapor is considered as the most promising method for the elimination of NH_3 from oxygen-containing exhaust gases (Equation (1)) [7]:

$$4\ NH_3 + 3\ O_2 \rightarrow 2\ N_2 + 6\ H_2O \quad (1)$$

NH_3 is generated by an onboard aqueous urea dosing system. The obtained ammonia acts as a NO_x reductant in the $DeNO_x$ process. There is a serious risk that unreacted ammonia is released into the atmosphere. Thus, the active SCO catalysts (so-called *guard catalyst*, ammonia slip catalyst—ASC, ammonia oxidation catalyst—AMOX) should operate in a broad temperature range (up to 600–700 °C—in the cycle of diesel particulate filter regeneration) in the presence of typical components of the exhausts (H_2O, CO_x, and SO_x), and additionally should selectively direct the reaction to the formation of N_2 and H_2O. Euro VI emission standards for heavy-duty vehicles (HDVs) introduced for the first time limits for NH_3 emissions up to 10 ppm [8]. Currently, there are no limits for NH_3 emitted from light-duty vehicles (LDVs, i.e., passenger cars), despite their high levels of emissions (e.g., [9,10]). Thus, potentially NH_3 will be considered next to ultra-fine particles smaller than 23 nanometers (PN_{10}) and nitrous oxide (N_2O) in the upcoming regulations, e.g., upcoming Euro emission standards.

Various kinds of catalysts were studied for NH_3-SCO, including noble metals (e.g., Ru [11]), supported noble metals (e.g., Au/Nb_2O_5, Au/ZrO_2 [12]), (mixed) metal oxides, supported metal oxides, modified zeolites (e.g., Pt-$CuMgAlO_x$ [13], Ag-USY [13]), etc. These groups of catalysts investigated in NH_3-SCO were summarized by Jabłońska et al. [7,14], Gao et al. [15] and Lan et al. [16]. In general, noble metal-based catalysts tend to possess high activity at low temperatures (< 300 °C), while their high cost and relatively low N_2 selectivity have restrained their widespread application. Transition metal-containing oxides and zeolites show improved selectivity toward N_2 than noble metal-based catalysts; however, they need higher operating temperatures (300–600 °C). Consequently, the proper combination of these two metals (in the form of bifunctional catalysts) could produce the catalysts with enhanced activity and N_2 selectivity. In general, the concept of bifunctional catalysts is based on the internal selective catalytic reduction (i-SCR) mechanism. This mechanism consists of two main steps. In the first step, part of ammonia is oxidized to NO and NO_2—minor by-product, while in the second step, NO and NO_2 are reduced by ammonia (unreacted in the first step) with the formation of N_2 and H_2O ($DeNO_x$, NH_3-SCR). In this step, also the formation of N_2O is possible. Besides the i-SCR mechanism, other major reaction pathways, i.e., the imide (NH, in which NH_3 transforms to N_2 and N_2O as final products, with nitrosyl (HNO) as an intermediate) mechanism and the hydrazine (with the formation of a hydrazine-type (N_2H_4) intermediate) mechanism were proposed for NH_3-SCO over different types of catalysts. The details of the above-mentioned reaction mechanisms can be found in previous review articles (e.g., [7,14]). Additionally, due to lack of identification of the characteristic intermediates of the aforementioned three mechanisms, recently Wang et al. [17] proposed a N_2^- mechanism of NH_3-SCO on a Ag/nano-Al_2O_3. Li et al. [18] postulated an Eley–Ridel mechanism over perovskite-based catalysts, where gaseous NH_3 reacts with adsorbed -ONH_2 species to form the surface diazo species (-N=N-) with the rate-determining step depending on the catalysts composition.

Recent interest focuses on bifunctional catalysts consisting of noble metal-based catalyst and transition metal-based catalyst. Previous review articles, including ammonia oxidation, give a clear statement about high activity, N_2 selectivity, and stability over Cu-containing materials (Jabłońska et al., 2016, Jabłońska, 2020) [7,19]. From the noble metal-based catalysts the most frequently applied—Pt/Al_2O_3, provides high activity but also significant selectivity to byproducts (N_2O and NO_x). Besides Pt/Al_2O_3, also the Ag/Al_2O_3 catalyst has received extensive concerns on the low-temperature NH_3-SCO. Other systems were less investigated for NH_3-SCO than Pt/Al_2O_3 or Ag/Al_2O_3. Thus, the present mini-review aims to provide a broad picture of the property-activity correlations of no-

ble metal-based catalysts investigated for NH_3-SCO up to now (including Pt-, Pd-, Ag- and Au-, Ru-based catalysts). The NH_3-SCO catalysts are classified considering their full NH_3 conversion and N_2 selectivity in the same temperature range. If not provided in the references, the catalytic activity and N_2 selectivity were roughly estimated based on NH_3 conversion-temperature profiles. This overview will shed light on future research directions regarding catalyst composition and architecture that maximizes the oxidation of NH_3 into N_2 over a broad temperature range and in the presence of the typical components of exhaust, such as H_2O, SO_x, and CO_x.

2. Pt- and Pd-Based Catalysts

Early work on NH_3 oxidation was given by Il'chenko et al. [20] Among metal-based catalysts, Pt and Pd are the most active for the ammonia oxidation (p(NH_3) = 0.1 atm, p(O_2) = 0.9 atm) but also the most selective to N_2O—according to the following order: Pt, Pd > Ni > Fe > W > Ti (note that Rh was not mentioned in Il'chenko review). The catalytic ammonia oxidation over platinum is a key step in the industrial manufacturing of nitric acid. The ammonia oxidation exhibits a moderate structure sensitivity, while the activity decreased in the order of: Pt foil > Pt(865) > Pt(533) > Pt(443) > Pt(100) due to different oxygen sticking coefficient [21]. Novell–Leruth et al. [22] used periodic slab density functional theory (DFT) calculations and found that NH_3 adsorbs preferentially on the top sites, NH_2 (dehydrogenation intermediates) on the bridge sites, while NH and N species on the hollow sites on both the (111) and (100) surfaces. The ammonia oxidation with atomic or molecular oxygen over Pt(100), Pt(111), stepped Pt(111)/Pt(211) or terrace Pt(111) orientations, etc., yields N_2, NO, N_2O, and H_2O, in varying amounts depending on reactant conditions. Steady-state reaction studies [23] under ultra-high vacuum (UHV) conditions with a stepped Pt(111) surface revealed that excess NH_3 lead to N_2 formation, while under excess O_2, NO formation was preferred. No other nitrogen-containing products, i.e., N_2O were detected in the gas phase (note that N_2O was never observed under UHV conditions [24]). Similar conclusions were given by Pérez–Ramirez et al. [25], who studied the sequence of steps in NH_3 oxidation (applying the isotope $^{15}NH_3$) over Pt, Pd, and Rh wires in the temporal analysis of products (TAP) reactor at relevant temperatures in industrial ammonia burners. High NO selectivity is favored at a high ratio of adsorbed $n(O)/n(NH_x)$ species, e.g., at $c(O_2)/c(^{15}NH_3) = 0.1$, the ^{15}NO selectivity over Pt reached 45%, while at $c(O_2)/c(^{15}NH_3) = 10$—ca. 100% selectivity. NO was found to be a primary reaction product in NH_3 oxidation, while N_2 and N_2O originate from consecutive NO transformations. Pd and Rh were more active for the reduction of nitric oxide by ammonia than Pt (Figure 1). Additionally, DFT calculations showed that the N_2O formation over Rh(100) plane needs higher activation energy than over Pt(100) or Pd(100). Furthermore, Rh(100) was more active in NH_3 decomposition (possessed a lower activation barrier for the $NH_3 \rightarrow NH_2$ step) than Pt and Pd surfaces, and strongly stabilized the dehydrogenated NH and N species [22].

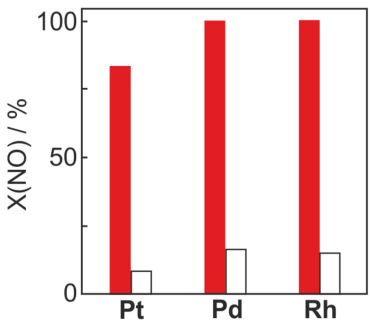

Figure 1. Conversion of NO over the PGMs on pulsing of $c(^{15}NH_3)$:c(NO):c(Ne) = 1:0.2:1 (solid bars) and $c(^{15}NH_3)$:c(NO):c(Ne) = 1:2:1 (open bars) at 800 °C. Reprinted from [25] with permission from Elsevier.

γ-Al_2O_3 and ZSM-5 are often used as the supports for noble metal-based catalysts for the selective catalytic oxidation of NH_3. A summary of Pt-, Pd-based catalysts is presented in Table 1. Pt/Al_2O_3 is usually applied to provide high low-temperature activity. The main drawback of such catalyst is low N_2 selectivity due to the formation of N_2O (below 250 °C) and NO_x (above 250 °C). The metallic Pt is significantly more active for NH_3-SCO than oxidized platinum [26,27], which provide limited sites for O_2 dissociation [28]. The operando XANES/EXAFS studies revealed the highest N_2 selectivity (ca. 80%) over H_2-reduced (2 wt.%)Pt/Al_2O_3. Nevertheless, under reaction conditions, at least 40% of Pt surface remains oxidized resulting in the formation of N_2O [29]. Otherwise, the metal-support interactions of Pt/TiO_2 were reported to stabilize Pt in the metallic state (also under reaction conditions) [30]. The Pt^0 content can also be manipulated by preparation procedure of Pt/SiO_2-Al_2O_3, i.e., by adding ascorbic acid (vitamin C, vC; n(vC)/n(Pt) = 0.25–1.5) [31]. Ostermaier et al. [26] reported that small Pt particles (2.0 and 2.7 nm) of (1–2.93 wt.%)Pt/Al_2O_3 demonstrate lower activity in comparison to larger crystallites (15.5 nm). The catalysts with a small size of Pt^0 crystallites were characterized by the strongest deactivation during NH_3 oxidation due to their oxidation to PtO_x, where x depends on the particle size [32]. Later, Sobczyk et al. [33,34] demonstrated with positron emission profiling (PEP) that the catalysts deactivate due to poisoning of the surface mainly by nitrogen species (NH and NH_2).

The dispersion of Pt species was increased after the introduction of ethylenediamine (from 2.8 to 2.0 nm) during the preparation of (1 wt.%)Pt/SiO_2-Al_2O_3 [35], and thus lead to higher activity in NH_3-SCO in the presence of CO_2 and H_2O, compared to that of unmodified samples. The N_2 selectivity remained nearly unaffected by the Pt particle size. Contrary to these studies, Slavinskaya et al. [36] found that a larger Pt particle size (ca. ~23 nm compared to ~1 nm) of (2 wt.%)Pt/Al_2O_3 enhanced activity. Additional measurements in the presence of CO_2 and H_2O did not change the trends of activity and selectivity of Pt/Al_2O_3 on the Pt dispersion and Pt state. Similar to the above discussed studies over Pt/SiO_2-Al_2O_3, N_2 selectivity did not depend on the Pt particle size, while in all cases, N_2 selectivity was below 70% (>300 °C). Furthermore, authors [27] showed no deactivation of the catalysts, i.e., the oxidation state of platinum in Pt/Al_2O_3 did not increase after the catalytic experiments. Also, the hydrothermal aging (in a feed containing O_2, H_2O, CO_2, at 550 °C over 250 h) of a Pt/Al_2O_3 washcoated monolith did not influence its activity below 250 °C [37]. Above 300 °C the activity significantly decreased with aging time (0, 122, 253 h) but the product selectivity remains the same. Recently, Machida et al. [38] found that a thin-film catalyst, which was prepared by deposing a nanoscale-thickness Pt(111) overlayer on a 50 μm-thick Fe-Cr-Al metal foil (Pt/SUS) achieved more than 180-fold higher TOF compared with the conventional (0.13 wt.%)Pt/Al_2O_3. The thermal stability of Pt/SUS was enhanced by the insertion of the Zr layer between the Pt and SUS foil. For the Pt surfaces, the NH mechanism was mostly proposed by experimental and DFT simulation studies; e.g., over Pt(100) or Pt(111) [39–41]. Also, the so-called *NH mechanism* (i.e., NH as the intermediates in the imide mechanism) occurred on Pt/Al_2O_3, while the *HNO and N_2H_4 mechanism* (i.e., HNO and N_2H_4 as the intermediates in the imide and hydrazine mechanism, respectively) coexisted on Pt/$CeZrO_2$ (Figure 2) [42].

Li and Armor [43] studied a series of zeolite ZSM-5 ion-exchanged with (4.07 wt.%)Pd, (2.66 wt.%)Rh, and (2.55 wt.%)Pt as catalysts for NH_3-SCO. Among them, relatively high activity and N_2 selectivity in the low-temperature range (≤300 °C) were found for the Pd-containing catalysts (i.e., full ammonia conversion with 91% N_2 selectivity at 300 °C in the presence of 5 vol.% H_2O). 58–61% of N_2O selectivity on (2.55 wt.%)Pt-ZSM-5 and 16–25% on (4.01 wt.%)Pd-ZSM-5 was obtained at 250–300 °C. The noble metal-exchanged ZSM-5 materials were less affected by water vapor than the corresponding Al_2O_3 supported catalysts. Similar results, i.e., 92% NH_3 conversion and 73% N_2 selectivity at 350 °C over (5.51 wt.%)Pd-ZSM-5 in NH_3-SCO (feed without H_2O), were also reported by Long and Yang [44]. Furthermore, Jabłońska et al. [45] investigated zeolites HY modified with palladium (0.05–2.5 wt.%). An increase in Pd loading leads to higher catalysts activity

together with the drop in N_2 selectivity. The palladium oxide species (PdO_x) were found to be active sites for ammonia oxidation (based on FT-IR studies). A part of ammonia was stabilized against oxidation over the zeolite framework acid sites (in the form of NH_4^+), and lead to enhanced N_2 selectivity in the higher temperature range. The analysis of the results of temperature-programmed (NH_3-SCO with various spaces velocity) and spectroscopic studies lead to the conclusion that the ammonia oxidation over Pd-Y followed the i-SCR mechanism. On the other hand, an appearance of hydrazine species (intermediates in the hydrazine mechanism) on the ammonia pre-adsorbed Pd-Y catalyst at 250 °C during FT-IR studies, suggested that the ammonia oxidation is more complicated and followed different parallel routes. Otherwise, Wells et al. [46,47] identified PdN_x under reaction conditions over H_2-reduced (1.5 wt.%)Pd/Al_2O_3 and Pd/Y (n(Si)/n(Al) = 2.6) as the dominant species during N_2 formation (based on combined operando spectroscopy and DFT calculations). As stated above, palladium-containing materials appear as promising NH_3-SCO catalysts, although, their stability (also in the presence of H_2O, SO_x, and CO_x) needs confirmation.

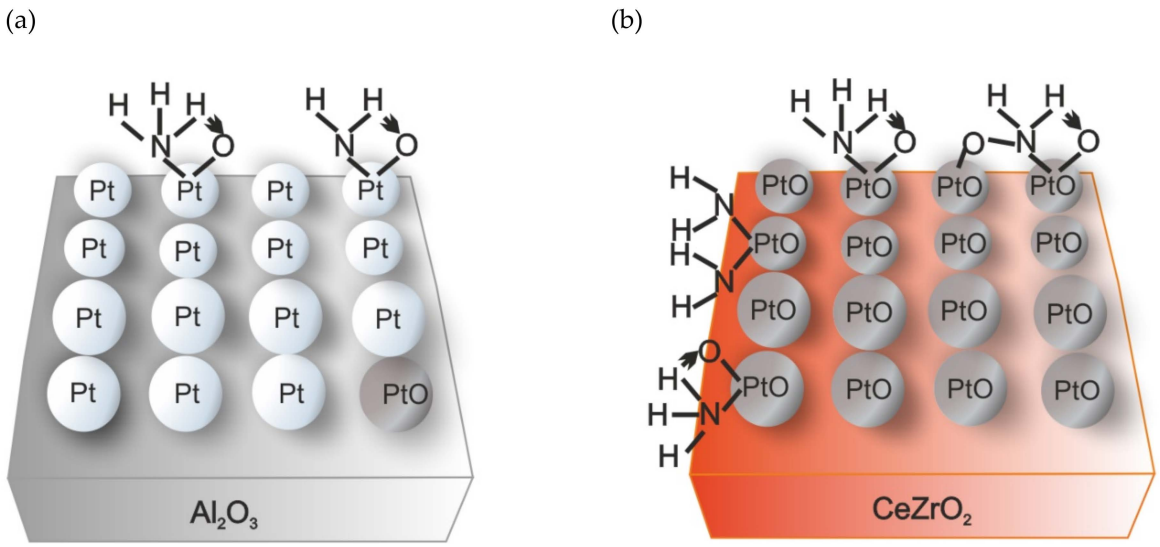

Figure 2. (**a**) Reaction mechanisms and Pt states over Pt/Al_2O_3 and (**b**) Pt/$CeZrO_2$. Reprinted from [42] with permission from ACS Publications.

The state-of-the-art NH_3-SCO systems include a combination of a noble metal-based catalyst—usually Pt/Al_2O_3, and an SCR catalyst, e.g., Cu- or Fe-containing zeolite. Thus, a part of ammonia is oxidized over the noble metal-based catalyst to N_2 and NO_x which is further transformed to N_2 over the SCR catalyst. Different arrangements of both metals were reported in the literature, i.e., noble/transition metal deposited on one support in systems such as (0.05 wt.%)Pt/(1 wt.%)Cu/Al_2O_3 [48], (0.5–4 wt.%)Pt/(20 wt.%)Cu/Al_2O_3 [49], (1 wt.%)Pt/(20 wt.%)Cu/Al_2O_3 [50–52], (1.5 wt.%)Pt-(5.5 wt.%)Cu/ZSM-5 [53], (0.5 wt.%)Pt-(1.54 wt.%)Fe-ZSM-5 [54], (1.5 wt.%)Pt-(0.5 wt.%)Fe/ZSM-5 [55], (0.21 wt.%)Pt/$CuMgAlO_x$ hydrotalcite-derived mixed metal oxides [13], (2 wt.%)PdO/(5 wt.%)CuO/Al_2O_3 [56], etc. Besides such form, the active components may be present in different configurations—dual-layer configuration, mixed and hybrid layer sample types, that are presented in Figure 3. The dual-layer catalytic systems consist of noble metal-based catalyst as a bottom layer, and transition metal-based catalysts as an upper layer, i.e., Pt/Al_2O_3 and Cu-ZSM-5, Pt/Al_2O_3 and Cu-SSZ-13, Pt/Al_2O_3, and Fe-ZSM-5 investigated by Shrestha et al. [57–59], Pt/Al_2O_3 and Fe-zeolite investigated by Scheuer et al. [60] and Colombo et al. [61]. E.g., Shrestha et al. [57] pointed out the increase of N_2 selectivity (with a corresponding decrease in NO selectivity) with increasing copper loading of Cu/ZSM-5 (NH_3-SCR layer), e.g., from 58% to 82% at 250 °C for 0.8 and 2.5 wt.% of Cu, respectively. Still, N_2O selectivity reached a maximum of about 40% at 260 °C in all

cases. Similar N_2O selectivity was reported over Pt/Al_2O_3 and Fe-ZSM-5 arranged as both dual-layer and mixed catalysts [58]. Also, the NH_3 oxidation depended on the applied conditions, i.e., space velocity (66,000 *versus* 265,000 h^{-1}). At higher space velocity mixed catalyst revealed (ca. 7%) higher NH_3 conversion, while dual-layer catalyst provided higher N_2 selectivity (especially above 350 °C). The hybrid catalyst (bottom layer of mixed Cu-SSZ-13 + Pt/Al_2O_3, top layer of Cu-SSZ-13) allowed to achieve (ca. 5%) higher NH_3 conversion than that of the dual-layer catalyst [59]. Furthermore, Dhillon et al. [62] applied sacrificial agents (yeast or polymer) to generate macropores on a (2.90 wt.%)Cu-SSZ-13 top-layer washcoat supported on (1.47 wt.%)Pt/Al_2O_3, and thus to enhance NH_3 conversion (still below 90% up to 500 °C) without impact on N_2 selectivity. Recently, Gosh et al. [63] reported a Pt/Al_2O_3@Cu-ZSM-5 (0.05 wt.% Pt, 2.93 wt.% Cu) core-shell catalyst that allowed full NH_3 conversion at ca. 300 °C and 100% N_2 selectivity (up to 275 °C). The NH_3 conversion was negligibly affected by the variation in the shell thickness (0.5 µm *versus* 1.2 µm), while the ticker shell was beneficial in improving N_2 selectivity at higher temperatures. The addition of H_2O (5 vol.%) to the feed had a minor impact on the catalyst activity, while more tests in the presence of CO_x and SO_x are still required.

Concluding this part, as can be seen from the above presented data, a great variety of Pt- and Pd-based catalytic systems were developed and tested for NH_3-SCO. In particular, (1–2 wt.%)Pt/Al_2O_3 was reported as one of the most active catalyst that allowed to obtain full NH_3 conversion around 200–450 °C with N_2 selectivity of 15–87% (according to data gathered in Table 1), depending on the applied catalyst preparation procedure as well as pretreatment and reaction conditions. Pt^0 serves as the active species responsible for high catalytic activity, and thus most of the catalytic systems were prepared by an impregnation method and subsequently reduced in H_2. Great research efforts aimed at determining the role of Pt dispersion in NH_3-SCO, but there is no clear consensus about it yet. Platinum (0.05–1.5 wt.%) was also applied as the most active noble metal component in the bifunctional catalysts. Such systems fully oxidized NH_3 in a broad temperature range of 195–500 °C with 44–100% N_2 selectivity (according to data gathered in Table 1) depending on their architecture, i.e., Pt deposited on one support with transition metal component, as dual-layer catalysts, mixed form, hybrid catalysts or incorporated in the core-shell structure, etc. Among them the (0.46 wt.%)Pt/Al_2O_3-(2.5 wt.%)Cu-ZSM-5 dual-layer catalyst (full NH_3 conversion at 250–500 °C, 82–100% N_2 selectivity) and (0.05 wt.%)Pt/Al_2O_3@(2.93 wt.%)Cu/ZSM-5 core-shell catalyst (full NH_3 conversion at 310–500 °C, 91–94% N_2 selectivity) appear as the most interesting systems for further catalysts optimization. However, the stability of these catalysts and the influence of the potential catalyst pollutants usually present in the exhausts, i.e., H_2O, SO_x and CO_x, were not fully provided within the scope of the studies. A similar conclusion can be given for other Pt- or Pd-containing catalysts (only a few materials were tested in the presence of H_2O and CO_2). Hence, further studies are required to understand structure-activity relationships and reaction mechanisms under application-relevant reaction conditions.

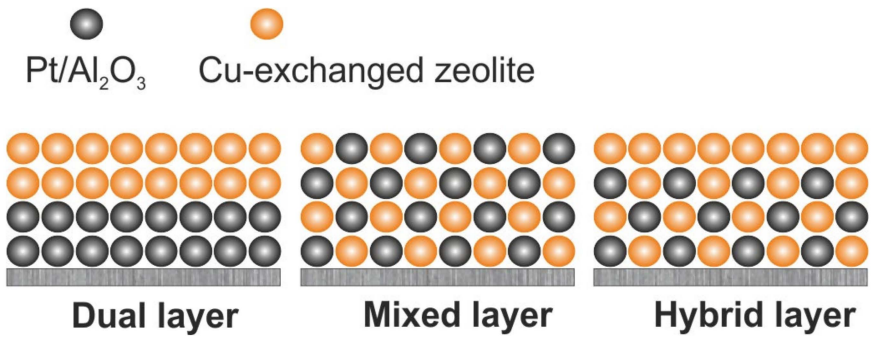

Figure 3. Schematic diagram representing bifunctional ammonia slip catalyst in three different washcoated structured methodologies. Reprinted from [64] with permission from Science Direct.

Table 1. Comparison of full NH_3 conversion and N_2 selectivity in same temperature range over Pt-based catalysts reported in literature.

Catalyst	Catalyst Preparation	Reaction Conditions	NH_3 Conversion_N_2 Selectivity/% (Temperature/°C)	Ref.
(3 wt.%)Pt-Rh	wash-coated on Al_2O_3, calcination, 400 °C, air	0.08 vol.% NH_3, 4 vol.% O_2, He balance, GHSV 92,000 h^{-1}	100/62% (400 °C)	[65]
(4.4 wt.%)Pt-Rh	wash-coated on Al_2O_3, calcination, 500 °C, air	0.1 vol.% NH_3, 4 vol.% O_2, He balance, GHSV 92,000 h^{-1}	100/80% (400 °C)	[66]
(1.2 wt.%)Pt/Al_2O_3	impregnation, calcination, 600 °C, air; reduction conditions not shown)	0.1 vol.% NH_3, 10 vol.% O_2, He balance, 50 mL min^{-1}, mass of the catalyst: 0.1 g, WHSV 30,000 mL h^{-1} g^{-1}	100/75% (200 °C)	[67]
		1.14 vol.% NH_3, 8.21 vol.% O_2, He balance, 74.7 mL min^{-1}, mass of the catalyst: 0.2 g, WHSV 22,410 mL h^{-1} g^{-1}	100/87% (200 °C)	
(1.73 wt.%)Pt/Al_2O_3	impregnation, calcination, 400 °C, air; reduction, 250 °C, H_2	0.1 vol.% NH_3, 4 vol.% O_2, He balance, 500 mL min^{-1}, mass of the catalyst: 0.145 g, GHSV 120,000 h^{-1}	100/40–60% (200–400 °C)	[27]
(2 wt.%)Pt/Al_2O_3	impregnation, calcination, 400 °C, air; oxidation, 400 °C, O_2/He	0.1 vol.% NH_3, 4 vol.% O_2, He balance, 500 mL min^{-1}, mass of the catalyst: 0.145 g, GHSV 120,000 h^{-1}	100/40–50% (325–400 °C)	[36]
	impregnation, calcination, 400 °C, air; reduction, 350 °C, H_2; calcination, 400 °C, Ar		100/30–60% (250–400 °C)	
(1 wt.%)Pt/Al_2O_3	impregnation, calcination, 550 °C, air	0.02 vol.% NH_3, 10 vol.% O_2, N_2 balance, 2.31 l min^{-1}, mass of the catalyst: 0.34 g, WHSV 407,000 mL g^{-1} h^{-1}	100/25–49% (250–450 °C)	[68]
(1 wt.%)Pt/CeO_2-SiO_2			100/15–42% (225–450 °C)	
(1 wt.%)Pt/SiO_2-Al_2O_3	impregnation, calcination, 550 °C, air; monolithic catalyst	0.02 vol.% NH_3, 10 vol.% O_2, 8 vol.% CO_2, 5 vol.% H_2O, N_2 balance, GHSV 100,000 h^{-1}	100/10–40% (300–450 °C)	[35]
(1 wt.%)Pt/SiO_2-Al_2O_3	impregnation; treatment strategies—conditions not shown; monolithic catalyst; Vc—ascorbic acid	0.02 vol.% NH_3, 10 vol.% O_2, 8 vol.% CO_2, 5 vol.% H_2O, N_2 balance, GHSV 100,000 h^{-1}	100/28–60% (240–300 °C)	[31]
(1 wt.%)Pt/SiO_2-Al_2O_3-vC			100/22–50% (240–300 °C)	
(1 wt.%)Pt/Al_2O_3	impregnation, calcination, 550 °C, air; monolithic catalyst	0.02 vol.% NH_3, 8 vol.% O_2, N_2 balance, GHSV 100,000 h^{-1}	100/15–30% (300–400 °C)	[42]
(1 wt.%)Pt/$CeZrO_2$			100/20–45% (325–400 °C)	
(1.5 wt.%)Pt/ZrO_2	impregnation, calcination, 550 °C, air	0.018 vol.% NH_3, 8 vol.% O_2, N_2 balance, GHSV 100,000 h^{-1}	100/25–60% (350–500 °C)	[53]
(1.5 wt.%)Pt-(5 wt.%)W/ZrO_2			100/28–50% (300–500 °C)	

Table 1. *Cont.*

Catalyst	Catalyst Preparation	Reaction Conditions	NH_3 Conversion_N_2 Selectivity/% (Temperature/°C)	Ref.
(2.0 wt.%)Pt/TiO_2	impregnation, calcination, 400 °C, air; oxidation, 400 °C, O_2/He	0.1 vol.% NH_3, 4.0 vol.% O_2, He balance, 500 mL min^{-1}, mass of the catalyst: 0.145 g, WHSV 206,897 mL h^{-1} g^{-1}	100/38–55% (200–400 °C)	[30]
	pulsed laser ablation in liquids, calcination, 400 °C, air oxidation, 400 °C, O_2/He		100/22–50% (175–400 °C)	
(0.1 wt.%)Pt/ (2 wt.%)V/TiO_2	impregnation, reduction, 600 °C, H_2/N_2	0.02 vol.% NH_3, 8.0 vol.% O_2, 6.0 vol.% H_2O, He balance, 500 mL min^{-1}, mass of the catalyst: 0.25 g, GHSV 60,000 h^{-1}	100/63–81% (250–350 °C)	[69]
(1.2 wt.%)Pd/Al_2O_3	impregnation, calcination, 600 °C, air; reduction—conditions not shown	1.14 vol.% NH_3, 8.21 vol.% O_2, He balance, 74.7 mL min^{-1}, mass of the catalyst: 0.2 g, WHSV 22,410 mL h^{-1} g^{-1}	100/98% (300 °C)	[67]
(4.2 wt.%)PdO/Al_2O_3	impregnation, calcination, 500 °C, air**reduction, 400 °C, H_2/He	0.1 vol.% NH_3, 4.0 vol.% O_2, He balance, * 0.1 vol.% NH_3, 4.0 vol.% O_2, 5 vol.% H_2O, He balance, 100 mL min^{-1}, mass of the catalyst: 0.1 g, WHSV 60,000 mL h^{-1} g^{-1}	100/67% (350 °C) ** 100/86% (300 °C)	[43]
(4.07 wt.%)Pd-ZSM-5	ion-exchange, calcination—conditions not shown		* 100/91% (300 °C)	
(1.5 wt.%)Pd/Y	impregnation, calcination—conditions not shown)	0.5 vol.% NH_3, 2.5 vol.% O_2, He balance, 40 mL min^{-1}, mass of the catalyst: 0.05 g, GHSV 15,400 h^{-1}	100/80–90% (250–500 °C)	[45]
(0.05 wt.%)Pt/ (1 wt.%)CuO/Al_2O_3	impregnation, calcination air, 600 °C; impregnation, calcination air, 500 °C	0.5 vol.% NH_3, 2.5 vol.% O_2, He balance, 40 mL min^{-1}, mass of the catalyst: 0.05 g, GHSV 15,400 h^{-1}	100/44–73% (325–500 °C)	[48]
(1 wt.%)Pt/ (20 wt.%)CuO/Al_2O_3	impregnation, calcination air, 500 °C; impregnation, calcination air, 450 °C	0.07 vol.% NH_3, 0.5 vol.% O_2, He balance*0.07 vol.% NH_3, 8 vol.% O_2, He balance1000 mL min^{-1}, WHSV 180,000 mL h^{-1} g^{-1}	100/88 (210–230 °C) * 100/95 (230 °C)	[49]
(4 wt.%)Pt/ (20 wt.%)CuO/Al_2O_3			100/83 (195–230 °C) * 100/90 (220–230 °C)	
(1.5 wt.%)Pt- (0.5 wt.%)Fe/ZSM-5	ion-exchange, calcination, air, 500 °C, impregnation calcination, air, 500 °C	0.1 vol.% NH_3, 2 vol.% O_2, He balance, 500 mL min^{-1}, WHSV 500,000 mL h^{-1} g^{-1}	100/61–88% (200–300 °C)	[55]
(0.5 wt.%)Pt- (1.54 wt.%)Fe/ZSM-5	ion-exchange, calcination, air, 500 °C, impregnation calcination, air, 500 °C	0.1 vol.% NH_3, 2 vol.% O_2, He balance, 500 mL min^{-1}, GHSV 230,000 h^{-1}	100/77–89% (250–400 °C)	[54]
(1.5 wt.%)Pt- (5.5 wt.%)Cu/ZSM-5	impregnation calcination, air, 550 °C	0.018 vol.% NH_3, 8 vol.% O_2, N_2 balance, GHSV 100,000 h^{-1}	100/56–73% (275–450 °C)	[53]

Table 1. *Cont.*

Catalyst	Catalyst Preparation	Reaction Conditions	NH_3 Conversion_N_2 Selectivity/% (Temperature/°C)	Ref.
(0.21 wt.%)Pt /$CuMgAlO_x$	impregnation, calcination, air, 500 °C	0.5 vol.% NH_3, 2.5 vol.% O_2, He balance, 40 mL min^{-1}, mass of the catalyst: 0.05 g, GHSV 15,400 h^{-1}	100/67–89% (350–500 °C)	[13]
(0.21 wt.%)Pd /$CuMgAlO_x$			100/71–76% (425–500 °C)	
(0.46 wt.%)Pt/Al_2O_3-(0.8 wt.%)Cu-ZSM-5	Pt/Al_2O_3: impregnation, calcination, 500 °C, air; reduction, 500 °C, H_2/Ar; Cu-ZSM-5: preparation not provided; oxidation, 650 °C, O_2/Ar; monolithic catalyst *dual layer catalyst	0.05 vol.% NH_3, 5 vol.% O_2, Ar balance, GHSV 66,000 h^{-1}	* 100/58–74% (250–500 °C)	[57]
(0.46 wt.%)Pt/Al_2O_3-(2.5 wt.%)Cu-ZSM-5			* 100/82–100% (250–500 °C)	
(0.46 wt.%)Pt/Al_2O_3-Fe-ZSM-5	Pt/Al_2O_3: impregnation, calcination, 500 °C, air, reduction, 500 °C, H_2/Ar, oxidation, 650 °C, O_2/Ar; Fe-ZSM-5: commercial; oxidation, 650 °C, O_2/Ar; monolithic catalyst *dual layer catalyst **mixed catalyst	0.05 vol.% NH_3, 5 vol.% O_2, Ar balance, GHSV 66,000 h^{-1}	* 100/48–93% (250–500 °C) ** 100/57–82% (250–500 °C)	[58]
(0.05 wt.%)Pt/ Al_2O_3@(2.93 wt.%)Cu/ ZSM-5	core-shell catalyst, Pt/Al_2O_3: impregnation, calcination, 550 °C, air; Cu-ZSM-5: ion-exchange, calcination, 500 °C, air	0.05 vol.% NH_3, 5 vol.% O_2, Ar balance, 100 mL min^{-1}, mass of the catalyst: 0.18 g, GHSV 280,000 h^{-1}	100/91–94% (310–500 °C)	[63]

3. Ag-Based Catalysts

Il'chenko et al. [20,70] reported that the specific activity of metal Ag at 300 °C was lower than that of Pt and Pd. Among silver-based catalysts, γ-Al_2O_3 impregnated with Ag species (mainly 10 wt.%) was widely investigated. Depending on the applied conditions, i.e., catalyst (its preparation, pre-treatment strategies, etc.) and reaction conditions, the full NH_3 conversion can be reached in the range of 150–400 °C with 45–95% N_2 selectivity over (10 wt.%)Ag/Al_2O_3 (according to data gathered in Table 2). However, at temperatures above 300 °C N_2 selectivity dropped due to the large NO production. For NH_3-SCO, the Ag/Al_2O_3 catalysts are mainly applied after H_2 pretreatment. E.g., gang et al. [71,72] reported extremely high activity of Ag/Al_2O_3 at 160 °C (full NH_3 conversion with N_2 selectivity of about 82%), which was even superior to H_2-reduced Ir/Al_2O_3 or Pt/Al_2O_3. The activity of Ag/Al_2O_3 was also higher than over silver powder and Ag/SiO_2 [72], indicating that the applied support influenced the Ag particle dispersion. However, the difference in the Ag particle size of the Ag/Al_2O_3 (8.2 nm) and Ag/SiO_2 (24 nm) catalysts was not discussed in these studies. The authors correlated the NH_3 oxidation activity at low temperatures to the catalysts' ability to promote dissociative or nondissociative adsorption of O_2. However, again the role of different oxygen species (i.e., adsorbed molecular

oxygen, adsorbed atomic oxygen, subsurface oxygen, and bulk dissolved oxygen) in the activity and the reaction mechanisms was not fully explored. Zhang and He [73] reported that the dissociation of O_2 is a rate-determining step for NH_3-SCO. They concluded that molecular O_2 can be dissociatively chemisorbed on the surface of H_2-reduced Ag/Al_2O_3, i.e., metallic species (in contrast to fresh material) to form O species, and thus enhance NH_3-SCO activity [74]. Furthermore, the modification of Ag/Al_2O_3 with CeO_2 improved catalysts' ability in the adsorption and activation of O_2 to form O species [75]. However, Wang et al. [76] claimed that the recovery of Brønsted acid sites via H_2 reduction (i.e., break of Ag-O bonds on the Ag/Al_2O_3 surface and formation of Ag clusters in the metallic state—$Ag_n{}^0$, based on EXAFS analysis) is also responsible for the improved activity of H_2-reduced Ag/Al_2O_3. Highly dispersed particles of Ag^0 (3.5–25 nm) were found to enhance the catalytic activity below 140 °C, whereas large particles (12–50 nm) of Ag^0 were responsible for improved N_2 selectivity [74].

Furthermore, N_2 selectivity of about 85% above 300 °C over (2.2 wt.%)Ag/Al_2O_3 ($c(NH_3)$:$c(O_2)$ = 1:1–1:25), was assigned to the small Ag particle size (<5 nm, based on XRD analysis) [77]. Ag^+ cations are the main active species in NH_3-SCO at temperatures above 140 °C. The adsorbed NH_3 mainly reacts with the gaseous O_2 over fresh Ag/Al_2O_3. Although besides Ag^0 and Ag^+, also $Ag_n{}^{\delta+}$ species were evidenced by DR UV-Vis analysis, the authors did not specify their role in ammonia oxidation. Also, Qu et al. [78] obtained highly dispersed Ag^0 particles with a size of 5–6 nm (based on XRD and DR UV-Vis analyses) on the H_2-reduced (10 wt.%) Ag/Al_2O_3 catalyst, which reached full conversion and 89% of N_2 selectivity at 180 °C. Yang et al. [79] and Jabłońska et al. [80] studied (1–10 wt.%)Ag/Al_2O_3 and claimed that the low N_2 selectivity above 200–300 °C over Ag/Al_2O_3 was ascribed to the formation of Ag_2O crystals.

Besides the influence of the Ag particle size, Wang et al. [17] investigated the effect of the different support particle size (micro-Al_2O_3 *versus* nano-Al_2O_3) on the activity of the final Ag/Al_2O_3 catalysts in NH_3-SCO. The catalyst characterization indicated that nano-Al_2O_3 was beneficial for Ag dispersion (the average Ag particle size of 3.7 nm, based on HRTEM analysis). The catalyst abundant acid sites (based on NH_3-TPD analysis) facilitated the adsorption and dissociation of NH_3, therefore resulting in an enhanced activity. Furthermore, the same research group [81] studied Ag supported on TiO_2, SiO_2 as well as their mixture—Ag/SiO_2-TiO_2. Although the (10 wt.%)Ag/SiO_2-TiO_2 catalyst reached full NH_3 conversion at 140 °C, N_2 selectivity in the whole studied range of 100–240 °C was below 70%. Significantly higher N_2 selectivity was obtained over Ag/TiO_2 (91–99% at 180–240 °C). Jabłońska et al. [82] compared commercial TiO_2 with mesoporous TiO_2 (prepared by evaporation induced self-assembly (EISA)) as support in NH_3-SCO. The activity and N_2 selectivity were favored over (1.5 wt.%)Ag-doped mesoporous TiO_2 (calcined at 600 °C, with predominant anatase phase). The easily reducible highly dispersed oxidized silver species were converted into Ag^0 and possibly $Ag_n{}^{\delta+}$ clusters through in situ H_2-pretreatment of catalyst. The metallic silver decomposed N_2O into N_2 and surface oxygen species, leading to higher N_2 selectivity. Further studies, concerning the stability tests, revealed that these materials are unstable, especially in the higher temperature range (>600 °C). However, temperature of the full conversion of NH_3 over (9.8 wt.%)Ag/Al_2O_3 also gradually increased after ca. 4 reaction cycles (from 150 to 250 °C). A higher stability in subsequent catalytic runs revealed (9.9 wt.%)Ag/ZSM-5 with the postsynthetic modified support. The micro-/mesoporous structure could prevent sintering and/or leaching of Ag particles during NH_3-SCO [83].

As stated above, while a broad number of studies examined NH_3-SCO over Ag-based catalysts, the mechanism of NH_3 oxidation and N_2 formation is still uncertain, and the studies are mainly based on temperature-programmed (TPD) or in situ DRIFTS studies. E.g., gang et al. [84] investigated NH_3-SCO over powder silver by TPD and in situ FT-Raman spectroscopy. They found NO as the main reaction intermediate yielding N_2O and/or N_2 (Figure 4a). The dissociation of oxygen was believed to be the rate-controlling step for ammonia oxidation, while low surface coverage favors N_2 formation. Similar

conclusions were given by Karatok et al. [85] The exposure of ozone on Ag(111) surfaces at −133 °C led to a disordered surface atomic oxygen overlayer (confirmed by LEED). Such oxygen species selectively catalyzed N-H bond cleavage, yielding mostly N_2 and minor amounts of by-products (NO and N_2O). Higher coverage O/Ag(111) surfaces at −133 °C led to bulk-like amorphous silver oxide species, forming NO and N_2O (Figure 4b). The ordered oxide surfaces—obtained through annealing of atomic oxygen-covered Ag(111) surface at 200 °C in UHV, showed only limited reactivity toward ammonia. Suppression of the N_2 formation at high oxygen coverages was also reported over Ir(510) and Ir(110) surfaces [86].

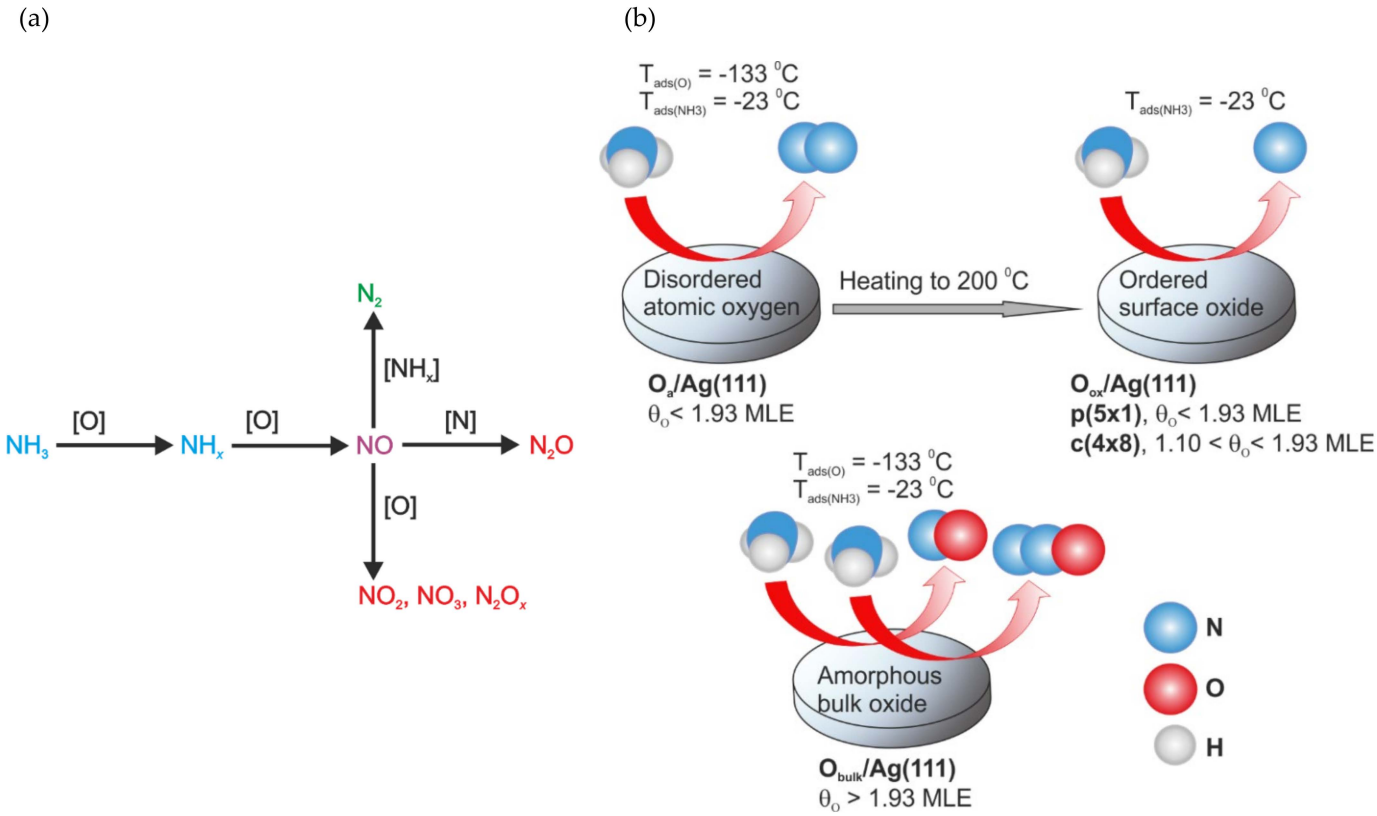

Figure 4. (**a**) Overall NH_3 reaction pathway on silver powder. Reprinted from [84] with permission from Elsevier; (**b**) reactivity and selectivity trends of NH_3-SCO on O/Ag(111) as a function of the oxygen coverage and temperature. Reprinted from [85] with permission from ACS Publications.

Zhang and He [73] investigated the reaction mechanisms over Ag/Al_2O_3 based on in situ DRIFTS studies and found that at low temperatures (<140 °C), NH_3 oxidation follows the -NH (imide) mechanism (Ag^0 as the main active species), while above 140 °C, NH_3 oxidation follows an in situ selective catalytic reduction (i-SCR) mechanism (Ag^+ as the main active species). Furthermore, they claimed that NH_3-SCO over Ag/nano-Al_2O_3 follows a reaction pathway called the N_2^- mechanism (based on in situ DRIFTS, kinetic measurements, and DFT calculation results) [17]. The intermediate N_2^- species appear from the combination of two -NH_2/NH species (considered to be the rate-determining step). In the next step, the N_2^- species are converted into N_2 and/or N_2O in the presence of O_2.

The activity and N_2 selectivity strongly depend on the loading of noble metal and can be steered into the desired direction by the introduction of transition metal. E.g., Yang et al. [79] studied Ag-Cu/Al_2O_3 with 5–5 or 10–10 wt.% of metal and indicated the material with the first composition as a highly efficient catalyst (full NH_3 conversion below 320 °C with N_2 selectivity of more than 95%). Unfortunately, the authors did not present results of catalytic tests above 350 °C. gang et al. [71] investigated (7.5 wt.%)Ag-(2.5 wt.%)Cu/Al_2O_3 and found the full conversion of ammonia at 200–300 °C with 95% N_2

selectivity. Above 300 °C appeared significant amounts of by-products—NO and N_2O. A mechanical mixture of (10 wt.%)Ag/Al_2O_3 and (10 wt.%)Cu/Al_2O_3—applied for comparative purposes, showed comparable activity and N_2 selectivity to a silver-based catalyst. The same oxidation state for bimetallic (Ag-Cu/Al_2O_3 (5–5 wt.%, 7.5–2.5 wt.%) and monometallic (10 wt.% Ag/Al_2O_3 or 10 wt.% Cu/Al_2O_3) catalysts were approved (based on XPS analysis). Additionally, LEIS analysis over (10–2.5 wt.%, 2.5–7.5 wt.%, 5–5 wt.%, 9–1 wt.%) Ag-Cu/Al_2O_3 excluded formation of any Ag-Cu phases. Jabłońska et al. [80] found among all tested combinations—1–1, 1–10, 1.5–10, 5–5 wt.% of silver and copper, respectively, the (1.5 wt.%)Ag-(10 wt.%)Cu/Al_2O_3 catalyst with an optimum activity, N_2 selectivity (full ammonia conversion and 94% N_2 selectivity at 375 °C) and stability in NH_3-SCO under wet conditions and time-on-stream tests. (0.59–2.34 wt.%)Ag-promoted $CuMgAlO_x$ hydrotalcite derived mixed metal oxides [87] with noble metal deposited inside the structure revealed relatively low NH_3 conversion below 350 °C. Silver loading of 2.34 wt.% (n(Ag)/n(Cu)/n(Mg)/n(Al) = 1/5/65/29) led to the formation of CuO_x and Ag_2O—that caused higher catalytic activity and the observed drop in N_2 selectivity. Significantly higher catalytic activity was reported for the Ag-Cu alloy nanoparticles (Figure 5a–d) synthesized by a solventless mix-bake-wash method. Ag-Cu (n(Ag)/n(Cu = 2/1, 77.25 wt.% of Ag) revealed full NH_3 conversion at 200 °C. The AgCu alloy structure maintains the metallic state of Ag and Cu as well as structure stability, which enhanced activity and thermal stability in NH_3 oxidation. The calcination of precursors of noble metal and transition metal did not form the alloy structure (Figure 5e–h). Besides, above-mentioned catalyst architectures, the (7.2 wt.%)Ag-(12.2 wt.%)Cu species were deposited onto wire-mesh honeycomb (WMH; characterized by open frontal area: 74.1%; geometric surface area: 16.2 cm^2 cm^{-3}; pressure drop: 2.58×10^{-2} Pa) [88]. Such catalyst revealed enhanced N_2 selectivity (above 89% at 180–320 °C) compared to Ag/WHM as well as stability in the presence of H_2 and CH_4.

Concluding this part, Ag-based catalysts (especially Ag/Al_2O_3) received extensive concerns in NH_3-SCO. As can be seen from the above examples, the research focuses mainly on the influence of the valance state of Ag species and particle size on the catalytic properties. As mentioned above, (10 wt.%)Ag/Al_2O_3 was suited for full NH_3 conversion at about 150–400 °C with 45–95% N_2 selectivity. Based on the presented above studies, the dispersed Ag^0 with an average particle size in the range between 3.5–6.0 nm was found as the active species for NH_3-SCO below 200 °C. On the other hand, there are limited studies that discuss the stability (especially concerning oxidation state) of the Ag-based catalysts, i.e., in the consecutive reaction cycles or the presence of H_2O, SO_x, and CO_x. Furthermore, despite their high potential, only a few studies addressed Ag-containing bifunctional catalysts for NH_3-SCO. A rather high content of Ag species (compared to Pt-based bifunctional catalysts, e.g., (7.5 wt.%)Ag-(2.5 wt.%)Cu/Al_2O_3 or (7.2 wt.%)Ag-(12.2 wt.%)Cu/WHM) was necessary to reach high activity and N_2 selectivity (i.e., full NH_3 conversion with 81–95% N_2 selectivity at 200–320 °C, according to data gathered in Table 2). The catalysts containing lower content of Ag species, i.e., 0.59–1.5 wt.% required a higher temperature of 375–500 °C to fully oxidize NH_3. Another important aspect of NH_3-SCO over Ag-based catalysts is the investigation of the reaction mechanisms, which were explored mainly by the application of in situ DRIFTS and the indication of the characteristic intermediates of the imide, hydrazine, or i-SCR (internal) mechanism. Overall, FT-IR investigations suggest that NH_3-SCO may follow different parallel pathways. Thus, the combination of the advantages of in situ DRIFTS with the advantages of other (e.g., temperature-programmed and/or transient) techniques will be strategic to clarify the pathways of NH_3-SCO. Furthermore, the exploration of the reaction mechanisms should be ongoing in the realistic catalytic mixture containing besides NH_3 and O_2 in the inert gas also H_2O, SO_x, and CO_x.

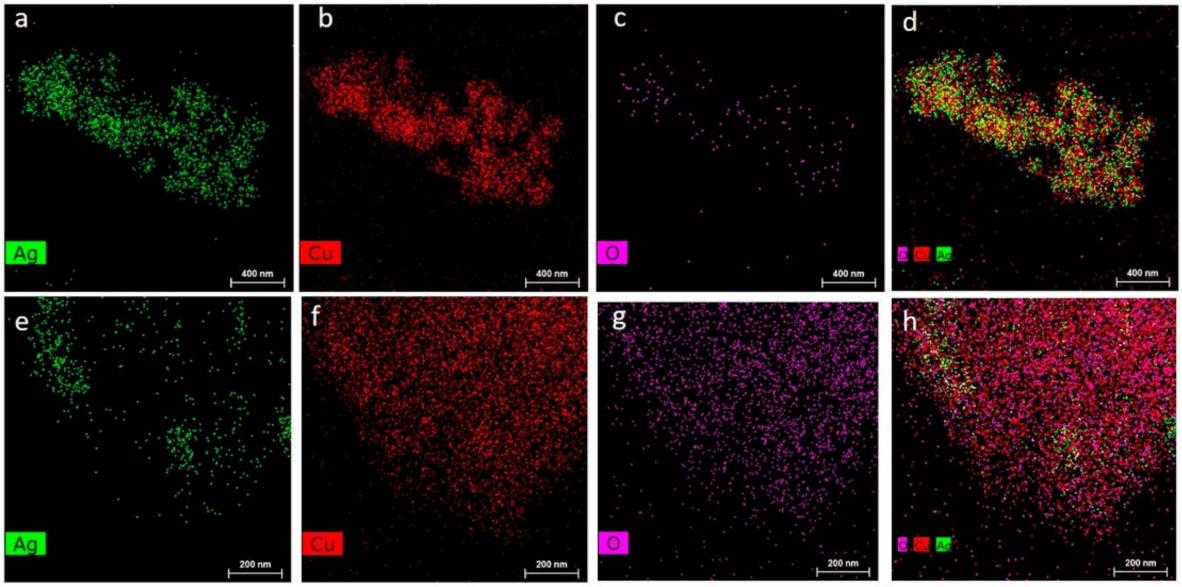

Figure 5. Energy-dispersive X-ray mapping for corresponding elemental distribution of Ag, Cu, and O on Ag_2Cu_1 (**a**–**d**) and $AgCuO_x$ NPs (**e**–**h**). Reprinted from [89] with permission from ACS Publications.

Table 2. Comparison of full NH_3 conversion and N_2 selectivity in same temperature range over Ag-based catalysts reported.

Catalyst	Catalyst Preparation	Reaction Conditions	NH_3 Conversion_N_2 Selectivity/% (Temperature/°C)	Ref.
Ag powder	Ag_2O, triple reduction, 400 °C, H_2/He; oxidation, 400 °C, O_2/He	0.1 vol.% NH_3, 10 vol.% O_2, 50 mL min^{-1}, mass of the catalyst: 0.1 g, WHSV 30,000 mL g^{-1} h^{-1}	100/33–77% (185–400 °C)	[72]
(10 wt.%)Ag/Al_2O_3	impregnation, calcination, 500 °C, air; reduction, 400 °C, H_2/He	0.1 vol.% NH_3, 10 vol.% O_2, 50 mL min^{-1}, mass of the catalyst: 0.1 g, WHSV 30,000 mL h^{-1} g^{-1}	100/70–88% (160–400 °C)	[72]
(10 wt.%)Ag/Al_2O_3	impregnation, calcination, 500 °C, air; *reduction, 400 °C, H_2/N_2	0.05 vol.% NH_3, 10 vol.% O_2, N_2 balance, 100 mL min^{-1}, GHSV 28,000 h^{-1}	100/93–95% (180 °C) *100/80–82% (160–180 °C)	[76]
(10 wt.%)Ag/Al_2O_3	calcination, 600 °C, air; reduction, 400 °C, H_2/N_2 impregnation	0.05 vol.% NH_3, 10 vol.% O_2, N_2 balance, 200 mL min^{-1}, mass of the catalyst: 0.2 g, WHSV 1000 mL h^{-1} g^{-1}	100/45–55% (150–200 °C)	[74]
	incipient wetness impregnation		100/55–60% (150–200 °C)	
	sol-gel		100/96% (300 °C)	
(10 wt.%)Ag/Al_2O_3	impregnation, calcination, 600 °C, air; reduction, 300 °C, H_2/N_2	0.1 vol.% NH_3, 10 vol.% O_2, N_2 balance, 400 mL min^{-1}, mass of the catalyst: 0.4 g, GHSV 50,000 h^{-1}	100/89 (180–260 °C)	[78]
(5 wt.%)Ag/Al_2O_3	impregnation, calcination, 600 °C, air	0.5 vol.% NH_3, 2.5 vol.% O_2, Ar balance, 40 mL min^{-1}, mass of the catalyst: 0.1 g, WHSV 24,000 mL h^{-1} g^{-1}	100/58–83% (275–500 °C)	[80]

Table 2. *Cont.*

Catalyst	Catalyst Preparation	Reaction Conditions	NH_3 Conversion_N_2 Selectivity/% (Temperature/°C)	Ref.
(10 wt.%)Ag/Al_2O_3	impregnation, calcination, 600 °C, air	1 vol.% NH_3, 10 vol.% O_2, He balance, 400 mL min^{-1}, mass of the catalyst: 0.8 g, WHSV 30,000 mL h^{-1} g^{-1}	100/70–83% (200–250 °C)	[79]
(10 wt.%)Ag/Al_2O_3	impregnation, calcination, 500 °C, air	1.14 vol.% NH_3, 8.21 vol.% O_2, 74.7 mL min^{-1}, mass of the catalyst: 0.2 g, WHSV 22,410 mL h^{-1} g^{-1}	100/83% (300 °C)	[71]
(1.5 wt.%)Ag/Al_2O_3	impregnation, calcination, 600 °C, air	0.5 vol.% NH_3, 2.5 vol.% O_2, Ar balance, 40 mL min^{-1}, mass of the catalyst: 0.1 g, WHSV 24,000 mL h^{-1} g^{-1}	100/78% (325 °C)	[82]
(10 wt.%)Ag/Al_2O_3			100/94% (225 °C)	
(2.2 wt.%)Ag/Al_2O_3	homogenous deposition precipitation, reduction, 400 °C, H_2	2 vol.% NH_3, 2 vol.% O_2, Ar balance, 40 mL min^{-1}, GHSV 2,500 h^{-1}*0.15 vol.% NH_3, 3.85 vol.% O_2, Ar balance, 40 mL min^{-1}, GHSV 2,500 h^{-1}	100/100% (368–400 °C) *100/85–100% (342–400 °C)	[77]
(1.6 wt.%)Ag /CeO_x/Li_2O/Al_2O_3			100/95–100% (275–400 °C)	
(10 wt.%)Ag /micro-Al_2O_3	impregnation, calcination, 500 °C, air	0.05 vol.% NH_3, 10 vol.% O_2, He balance, 100 mL min^{-1}, GHSV 28,000–115,000 h^{-1} *0.05 vol.% NH_3, 10 vol.% O_2, 5 vol.% H_2O, He balance, 100 mL min^{-1}, GHSV 136,000 h^{-1}	100/94–96% (160–180 °C)	[17]
(10 wt.%)Ag /nano-Al_2O_3			100/66–76% (120–180 °C) *100/74–90% (250–400 °C)	
(9.8 wt.%)Ag/Al_2O_3	rotary evaporator, calcination, 500 °C, air; reduction, 400 °C, H_2/Ar	0.1 vol.% NH_3, 10 vol.% O_2, He balance, 100 mL min^{-1}, GHSV 35,000 h^{-1}	100/70–74% (140–190 °C)	[83]
(9.9 wt.%)Ag/ZSM-5			100/82–89% (150–190 °C)	
(10 wt.%)Ag/SiO_2	impregnation, calcination, 500 °C, air; reduction, 400 °C, H_2/He	0.1 vol.% NH_3, 10 vol.% O_2, 50 mL min^{-1}, mass of the catalyst: 0.1 g, WHSV 30,000 mL h^{-1} g^{-1}	100/40–73% (200–400 °C)	[72]
(10 wt.%)Ag/SiO_2	impregnation, calcination, 600 °C, air; reduction, 300 °C, H_2/N_2	0.1 vol.% NH_3, 10 vol.% O_2, N_2 balance, 400 mL min^{-1}, mass of the catalyst: 0.4 g, GHSV 50,000 h^{-1}	100/50–63% (220–260 °C)	[78]
(10 wt.%)Ag/TiO_2			100/64% (260 °C)	
(10 wt.%)Ag/SiO_2	impregnation, calcination, 500 °C, air	0.05 vol.% NH_3, 10 vol.% O_2, N_2 balance, 100 mL min^{-1}, GHSV 28,000 h^{-1}	100/60–62% (180–240 °C)	[81]
(10 wt.%)Ag/TiO_2			100/91–99% (180–240 °C)	
(10 wt.%)Ag /SiO_2-TiO_2			100/60–70% (140–240 °C)	
(1.5 wt.%)Ag/mesoTiO_2	impregnation, calcination, 600 °C, air; *reduction, 600 °C, H_2/Ar	0.5 vol.% NH_3, 2.5 vol.% O_2, Ar balance, 40 mL min^{-1}, mass of the catalyst: 0.1 g, WHSV 24,000 mL h^{-1} g^{-1}	100/74–76% (375–400 °C) *100/81–87% (350 °C)	[82]
(10 wt.%)Ag/mesoTiO_2			100/81–87% (350–400 °C) *100/72–78(275–400 °C)	

Table 2. *Cont.*

Catalyst	Catalyst Preparation	Reaction Conditions	NH_3 Conversion_N_2 Selectivity/% (Temperature/°C)	Ref.
(7.3 wt.%)Ag/MnO_2	multi-step process, calcination, 400 °C, air	0.005 vol.% NH_3, 20 vol.% O_2, Ar balance *0.005 vol.% NH_3, 20 vol.% O_2, 0.057 vol.% H_2O, Ar balance 100 mL min^{-1}, mass of the catalyst: 0.15 g, WHSV 40,000 mL h^{-1} g^{-1}	100/98–99% (90–120 °C) *100/95–96% (115–130 °C)	[90]
(10 wt.%)Ag-Y	impregnation, calcination, 600 °C, air; reduction, 300 °C, H_2/N_2	0.1 vol.% NH_3, 10 vol.% O_2, N_2 balance, 400 mL min^{-1}, mass of the catalyst: 0.4 g, GHSV 50,000 h^{-1}	100/32–50% (220–260 °C)	[78]
(21 wt.%)Ag-Y	ion-exchange, calcination, 400–500 °C, air	0.5 vol.% NH_3, 2.5 vol.% O_2, He balance *0.5 vol.% NH_3, 2.5 vol.% O_2, 3.2 vol.% H_2O, He balance **0.5 vol.% NH_3, 2.5 vol.% O_2, 4.8 vol.% CO_2, He balance 40 mL min^{-1}, mass of the catalyst: 0.05 g, WHSV 48,000 mL h^{-1} g^{-1}	100/90% (300 °C)	[91]
(21 wt.%)Ag-USY			100/92–95% (200–300 °C) *100/98% (200–300 °C) **100/90–95% (200–300 °C)	
(33 wt.%)Ag-Y	ion-exchange, reduction, 400 °C, H_2	0.05 vol.% NH_3, 7 vol.% O_2, N_2 balance, 800 mL min^{-1}, mass of the catalyst: 0.25 g, WHSV 192,000 mL h^{-1} g^{-1}	100/70–80% (300–400 °C)	[92]
(5 wt.%)Ag-(5 wt.%)Cu/Al_2O_3	impregnation, calcination, 600 °C, air	1 vol.% NH_3, 10 vol.% O_2, He balance, 400 mL min^{-1}, mass of the catalyst: 0.8 g, WHSV 30,000 mL h^{-1} g^{-1}	100/95% (320 °C)	[79]
(7.5 wt.%)Ag-(2.5 wt.%)Cu/Al_2O_3	impregnation, calcination, 500 °C, air	0.1 vol.% NH_3, 10 vol.% O_2, He balance, 50 mL min^{-1}, mass of the catalyst: 0.1 g, WHSV 30,000 mL h^{-1} g^{-1}	100/95% (200–300 °C)	[71]
(10 wt.%)Ag/Al_2O_3+(10 wt.%)Cu/Al_2O_3 (mixture 3:1)	impregnation, calcination, 500 °C, air	1.14 vol.% NH_3, 8.21 vol.% O_2, 74.7 mL min^{-1}, mass of the catalyst: 0.2 g, WHSV 22,410 mL h^{-1} g^{-1}	100/82% (300 °C)	[71]
(1.5 wt.%)Ag-(10 wt.%)Cu/Al_2O_3	impregnation, calcination, 600 °C, air	0.5 vol.% NH_3, 2.5 vol.% O_2, Ar balance *0.5 vol.% NH_3, 2.5 vol.% O_2, 3.2 vol.% H_2O, Ar balance 40 mL min^{-1}, mass of the catalyst: 0.1 g, WHSV 24,000 mL h^{-1} g^{-1}	100/83–94% (375–500 °C) *100/83–94% (375–500 °C)	[80]
(0.59 wt.%)$AgCuMgAlO_x$	coprecipitation, calcination, 600 °C, air	0.5 vol.% NH_3, 2.5 vol.% O_2, Ar balance, 40 mL min^{-1}, mass of the catalyst: 0.1 g, WHSV 24,000 mL h^{-1} g^{-1}	100/88% (425–500 °C)	[87]
(2.34 wt.%)$AgCuMgAlO_x$			100/78–92% (400–500 °C)	
(77.25 wt.%)Ag-Cu nanoalloy	solventless mix-bake-wash method, 300 °C, air	0.1 vol.% NH_3, 10 vol.% O_2, N_2 balance, 100 mL min^{-1}, GHSV 12,000 h^{-1}	100/72–85% (210–240 °C)	[89]
(67.57 wt.%)$AgCuO_x$	calcination, 500 °C, air		100/64–72% (300–340 °C)	
(7.4 wt.%)Ag/WMH	WMH—wire-mesh honeycomb; impregnation, calcination, 500 °C, air	0.1 vol.% NH_3, 10 vol.% O_2, He balance, 300 mL min^{-1}, GHSV 2,250 h^{-1}	100/63–73% (210–320 °C)	[88]
(7.2 wt.%)Ag-(12.2 wt.%)Cu/WMH			100/81–89% (220–320 °C)	

4. Au- and Ru-Based Catalysts

Gold-based catalysts are well-known for their high catalytic activity at low temperatures, e.g., in the oxidation of CO [93,94]. However, such catalysts were rarely investigated in NH_3-SCO (Table 3). Interestingly, Lin et al. [95] investigated NH_3 oxidation over the in situ H_2-reduced (5 wt.%)Au/MO_x/Al_2O_3 (M = Cu, Fe, Ce, Li, and Ti) catalysts in the temperature range from 200 to 400 °C. Among all investigated catalysts, Au/Cu-Al_2O_3 was the most active and N_2 selective (full NH_3 conversion at 300 °C with 95% N_2 selectivity). The H_2-reduced Au/Al_2O_3 catalyst revealed significantly lower NH_3 conversion (ca. 30% above 400 °C). However, the NH_3 conversion increases with an increasing O_2 in the feed ($c(NH_3)$:$c(O_2)$ = 1:10; NH_3 conversion of 45% at 400 °C) [77]. gong et al. [96] and Liu et al. [97] reported from experimental and theoretical studies that NH_3 did not dissociate on the Au(111) surface until it was precovered with oxygen atoms or hydroxyl groups. Thus, Lippits et al. [77] observed the enhanced NH_3 conversion (full NH_3 conversion at 338 °C with N_2 selectivity below 50%) over Au/Al_2O_3 after its doping with CeO_x (able to provide and store oxygen) and Li_2O (responsible for decreasing the catalyst acidity and thus improved oxygen adsorption). Recently, Lin et al. [12] reported the acidic metal-oxide-supported gold catalyst (Au/Nb_2O_5) with improved N_2 selectivity compared to other metal-oxide-supported gold catalysts (e.g., Au/SiO_2, Au/Al_2O_3, Au/Fe_2O_3, etc., Figure 6a). Specifically, Au/Nb_2O_5 contains both Brønsted and Lewis acid sites that allowed NH_3 oxidation according to hydrazine mechanism (N_2H_4 as the intermediate) and imide mechanism (HNO as the intermediate), respectively (Figure 6b). Overall, further detailed property-activity studies over Au-containing materials could path the way for further catalysts design and their optimization.

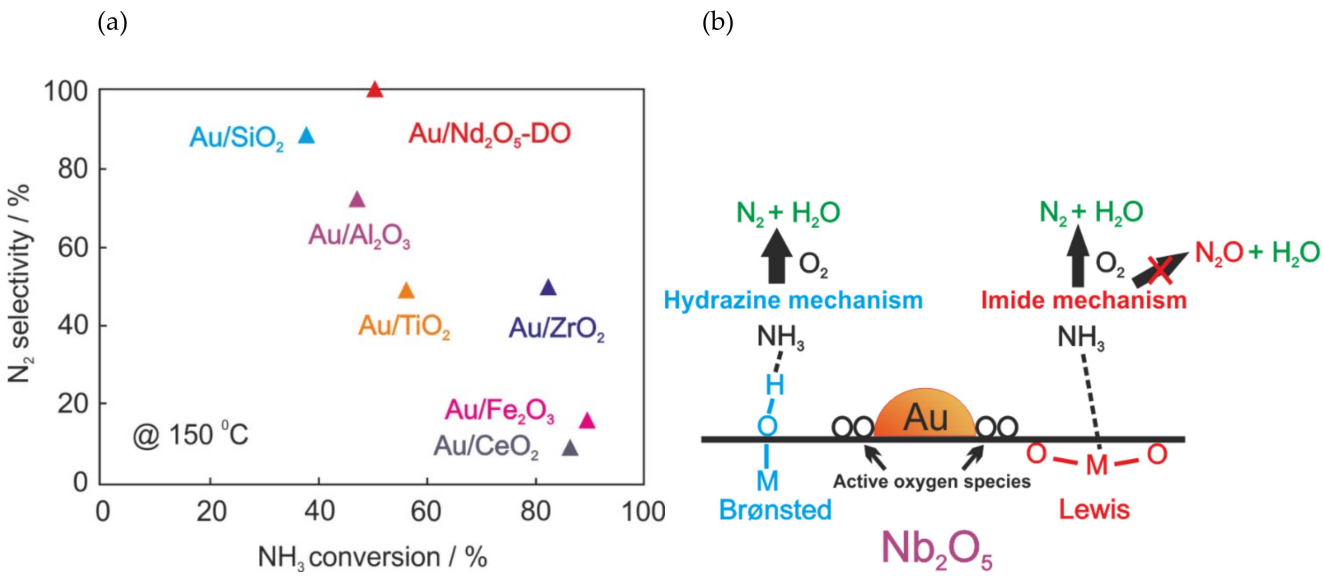

Figure 6. (**a**) NH_3 conversion and N_2 selectivity over Au/MO_x at 150°C. gold loading amount was 1 wt.%. Reaction conditions: a mass of catalyst, 0.15 g; 0.005 vol.% NH_3 and 20 vol.% O_2, Ar balance, GHSV 40 000 mL h^{-1} g^{-1}; (**b**) Suggested NH_3-SCO mechanisms of Au/Nb_2O_5. Reprinted from [12] with permission of ACS Publications.

Some studies were carried out on RuO_2(110) surface characterized by two types of atoms with unsaturated bonds along [1] direction: a) the twofold coordinated oxygen atoms (O-bridge; O-br) and b) the fivefold coordinated Ru atoms (Ru-cus; the adsorption site for ammonia) [98]. NH_3 decomposes (to NH_2) at −183 °C, while successive annealing to −23–27 °C produces N [98,99]. N_2 is predominantly formed over polycrystalline RuO_2 in a direct combination of Ru-coordinated N atoms (at ambient pressure, 6% of NO at $c(O_2)$:$c(NH_3)$ = 2:1; 65% of NO at $c(O_2)$:$c(NH_3)$ = 140:1) [100]. The selectivity to NO increases with increasing temperature (100% around 257 °C, in UHV, p(NH_3) = 10^{-7} mbar,

and $c(O_2)$:$c(NH_3)$ = 20:1) because of the high desorption temperature for NO (227 °C). At lower temperatures, NO-formation is hindered by surface water molecules [98,99]. Seitsonen et al. [99] estimated energy barriers to the elementary H-abstraction steps and the recombination of N and O atoms on RuO_2(110) surface by using DFT calculations and high-resolution core-level shift spectroscopy (Figure 7). The high activity of RuO_2(110) arose from low activation energies from the successive H-abstraction.

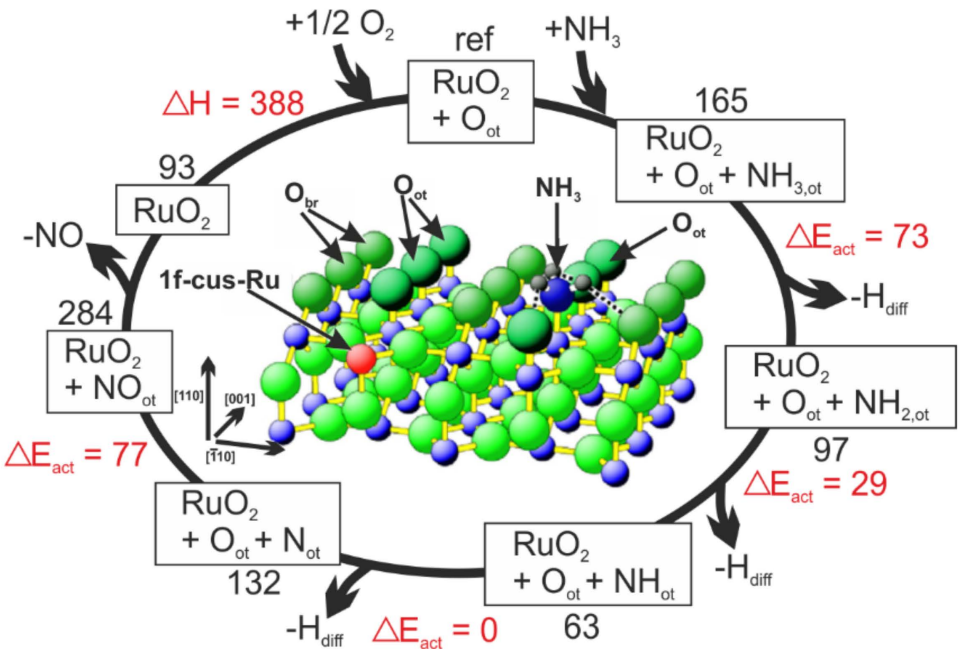

Figure 7. Microscopic reaction steps in NH_3 oxidation over RuO_2(110). Activation energies (red) and total adsorption energies (black) are determined by DFT calculations and are given in kJ mol^{-1}. -H_{diff} means that abstracted H from NH_x is removed from its direct neighborhood by diffusion along with various O species on the surface. Reprinted from [99] with permission from Elsevier.

Also, RuO_2-supported catalysts are active for ammonia oxidation (Table 3). E.g., Cui et al. investigated the RuO_2-CuO/Al-ZrO_2 [101] and CuO/RuO_2 [102] catalysts with 5–30 wt.% and 70–95 wt.% of Ru loading, respectively. The catalysts possessed excellent activity and N_2 selectivity at low temperatures, i.e., for (20 wt.%)RuO_2-CuO/Al-ZrO_2 full NH_3 conversion at 195 °C with 100% N_2 selectivity [101], or for (10 wt.%)CuO/RuO_2 full NH_3 conversion at 180 °C and N_2 selectivity above 95% [102] were achieved. However, these catalysts are relatively expensive and therefore their commercialization is hindered. Thus, Chakrobaty et al. [103] investigated the Cu/Ru catalysts with varying overlaying thickness of Cu film (with the optimum of 0.8 monolayers) deposited by physical vapor deposition on (5 nm)Ru/TiO_2 (111). The synergistic interaction between Cu and Ru species led to a threefold higher ammonia conversion rate than was achieved over Ru-based catalyst. Concerning the powder materials, Wang et al. [104] studied a series of WO_3-modified RuO_2-Fe_2O_3 catalysts with a lower cost, i.e., with 1 wt.% of ruthenium. The introduction of 5 wt.% of WO_3 (among 1–9 wt.% of WO_3) tuned the surface acidity, and thus, enhanced activity and N_2 selectivity of RuO_2-Fe_2O_3 (full NH_3 conversion at 250–400 °C and 93–97% N_2 selectivity). In situ DRIFTS results indicated that NH_3-SCO over (1 wt.%)RuO_2-(5 wt.%)WO_3-Fe_2O_3 proceeds according to the i-SCR mechanism. The -NH_2 intermediate reacted with the in situ-generated NO_x ad-species with the formation of N_2. Furthermore, Chen et al. [105,106] studied (0.2 wt.%)Ru/$Ce_{0.6}Zr_{0.4}O_2$(PVP) or (0.2 wt.%)IrO_2/$Ce_{0.6}Zr_{0.4}O_2$(PVP) (PVP, polyvinylpyrrolidone) and claimed that -HNO appeared as an intermediate in the i-SCR mechanism of NH_3-SCO (Figure 8). The formed -HNO interacted with atomic oxygen with the formation of NO, which furthermore reacts with -NH_x (-NH_2 and -NH) species with the formation of N_2 and N_2O (minor by-product).

The presence of SO_2 in the feed gas effectively inhibits the production of N_2O, i.e., the reactions between gaseous NO and -NH_2 will be enhanced (more adsorbed ammonia on the sulfated (acidic) surface). SO_2 can also inhibit NH_3 oxidation resulting in higher N_2 selectivity (up to 100%) in the absence of NO_x. Similar conclusions were given for RuO_x/TiO_2-SO_4^{2-}, however, the time of the sulfated treatment (0.5–6 h) of the support varied activity and N_2 selectivity of the final catalysts (with an optimum at 2 h) [107].

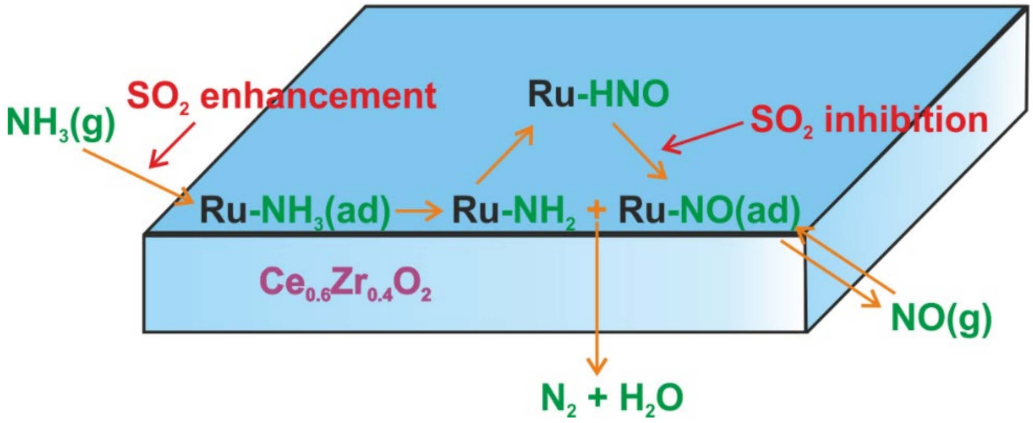

Figure 8. Mechanism of NH_3-SCO and effect of SO_2. Reprinted from [105] with permission of ACS Publications.

Concluding this part, both Au- and Ru-based catalysts were significantly less investigated in NH_3-SCO. A highly loaded Ru-containing materials (10–20 wt.% Ru; (10 wt.%)CuO-RuO_2 or (20 wt.%)RuO_2-CuO/Al-ZrO_2) present a class of highly active and N_2 selective catalysts at relatively low temperatures (i.e., full NH_3 conversion at 180–350 °C with 95–100% N_2 selectivity; according to data gathered in Table 3). Otherwise, the materials with significantly lower content of Ru species (0.5–3 wt.%) were less active (full NH_3 conversion at 175–400 °C) and N_2 selective (43–99%). However, again, concerning the influence of the preparation variables (e.g., the different total amount of ruthenium, variety of applied metal promoters and supports) as well as pretreatment and reaction conditions, the comparison of activity and N_2 selectivity over Ru-based catalysts each other or even with other noble metal-based catalysts is limited. Furthermore, for both Au- and Ru-based catalysts, oxidized metal species (i.e., Au^+/Au^{3+}, Ru^{4+}) ensure enhanced activity and N_2 selectivity (in contrast to the Pt- or Ag-based catalysts). Nevertheless, an in-depth understanding of the role of active species in NH_3-SCO is still lacking and needs to be demonstrated clearly in further studies (especially over Au-based catalysts). Furthermore, the presented catalytic systems were mainly investigated under ideal conditions (only NH_3 and O_2 diluted in inert gas) also concerning the investigation of the reaction mechanisms, i.e., through in situ DRIFTS experiments (NH_3 adsorption/desorption in inert gas or oxygen). Otherwise, surface reactions are fast (residence time in a range of seconds) and the reaction mechanism involves a series of parallel and consecutive reactions. Thus, the reaction intermediates and conversion of the substrate molecules on the catalyst surface should be followed with more detailed ex situ, in situ, and operando spectroscopic studies as well as transient kinetic investigations under-applied reaction conditions.

Table 3. Comparison of full NH_3 conversion and N_2 selectivity in same temperature range over Au- and Ru-based catalysts reported in literature.

Catalyst	Catalyst Preparation	Reaction Conditions	NH_3 Conversion_N_2 Selectivity/% (Temperature/°C)	Ref.
(5 wt.%)Au/CuO/Al_2O_3	impregnation, calcination, 300 °C, air; reduction, 300 °C, H_2	2 vol.% NH_3, 2 vol.% O_2, He balance, 30 mL min^{-1}, mass of the catalyst: 0.15 g, WHSV 12,000 mL h^{-1} g^{-1}	100/95% (300 °C)	[95]
(4 wt.%)Au/CeO_x/Li_2O/Al_2O_3	homogenous deposition precipitation, reduction, 400 °C, H_2	2 vol.% NH_3, 2 vol.% O_2, Ar balance, 40 mL min^{-1}, GHSV 2500 h^{-1}	100/34–49% (338–400 °C)	[77]
(10 wt.%)CuO-RuO_2	conanocasting-replication method, calcination, 500 °C, air	0.1 vol.% NH_3, 2 vol.% O_2, Ar balance, 100 mL min^{-1}, mass of the catalyst: 0.08 g, WHSV 75,000 mL h^{-1} g^{-1}	100/95–97% (180–350 °C)	[102]
(20 wt.%)RuO_2-CuO/ZrO_2	impregnation, calcination, 550 °C, air	0.04 vol.% NH_3, 5 vol.% O_2, 6 vol.% H_2O, Ar balance, 200 mL min^{-1}, mass of the catalyst: 0.1 g, WHSV 120,000 mL h^{-1} g^{-1}	100/68–98% (250–275 °C)	[101]
(20 wt.%)RuO_2/Al-ZrO_2			100/70–82% (248–325 °C)	
(20 wt.%)RuO_2-CuO/Al-ZrO_2			100/100% (195–280 °C)	
(1 wt.%)RuO_2-Fe_2O_3	sol-gel route, calcination, 500 °C, air	0.08 vol.% NH_3, 5 vol.% O_2, Ar balance, 400 mL min^{-1}, GHSV 60,000 h^{-1}	100/67–90% (250–400 °C)	[104]
(1 wt.%)RuO_2-WO_3-Fe_2O_3			100/93–97% (250–400 °C)	
(1.13 wt.%)Ru/Cu-SSZ-13	impregnation, 500 °C, air; pretreatment, 300 °C, O_2/N_2	0.05 vol.% NH_3, 0.5 vol.% CO, 5 vol.% O_2, N_2 balance, GHSV 300,000 h^{-1}	100/94–96% (220–300 °C)	[108]
(3 wt.%)RuO_2/TiO_2	impregnation, calcination, 400 °C, air	0.1 vol.% NH_3, 5 vol.% O_2, 3 vol.% H_2O, N_2 balance, 150 mL min^{-1}, mass of the catalyst: 0.1 g, WHSV 90,000 mL h^{-1} g^{-1}	100/47–72% (350–400 °C)	[109]
(3 wt.% Ru)RuO_2/Na-Y	ion-exchange, pretreatment, 450 °C, O_2/H_2O/N_2		100/51–99% (175–400 °C)	
(1 wt.%)Ru/TiO_2	impregnation, 400 °C, air; pretreatment, 400 °C, O_2/N_2	0.02 vol.% NH_3, 10 vol.% O_2, 6 vol.% H_2O, N_2 balance, 500 mL min^{-1}, mass of the catalyst: 0.3 g, GHSV 60,000 h^{-1}	100/54–63% (275–300 °C)	[110]
(0.5 wt.%)Ru/TiO_2	impregnation, 450 °C, air; pretreatment, 400 °C, O_2/N_2	0.08 vol.% NH_3, 5 vol.% O_2, N_2 balance, 400 mL min^{-1}, GHSV 60,000 h^{-1}	100/43–85% (200–400 °C)	[107]
(0.5 wt.%)Ru/TiO_2-SO_4^{2-}			100/65–93% (225–400 °C)	

5. Conclusions and Outlook

NH_3-SCO is the most efficient method for ammonia removal from oxygen-containing exhausts. The number of publications related to this process successively increases with the main researchers' interest in the development of the catalyst with high activity, N_2 selectivity, and stability in the broad temperature range. The present mini-review provides a broad picture of the property-activity correlations of noble metal-based catalysts investigated for NH_3-SCO. Among presented Pt-, Pd-, Ag- and Au-, Ru-based catalytic systems, mainly H_2-reduced (1–2 wt.%)Pt/Al_2O_3 and (10 wt.%)Ag/Al_2O_3 were recognized as the most active NH_3-SCO systems in the low temperatures (<300 °C). Unfortunately,

they caused significant formation of N_2O and NO_x. Moreover, as can be seen from the above examples, although Pt- and Ag-based catalysts were more intensively investigated regarding their property-activity correlations—compared to that of the Pd-, Au-, and Ru-containing catalysts—there is still a lack of systematic studies concerning the nature and role of active species as well as the influence of (a) the particle size of active components and their aggregation state; (b) the catalyst supports (i.e., inorganic oxides versus zeolites); (c) the preparation methods (i.e., catalysts in the structured forms, e.g., monolith), and (d) feed composition (i.e., various $c(NH_3)$:$c(O_2)$ ratios (1:1–25—an excess of oxygen together with minor NH_3 slip, presence of H_2O, SO_x, CO_x, etc.) on activity, N_2 selectivity, and stability in catalysis. Contrary to the transition metal-based catalysts only a few examples concern catalytic studies over noble metal-based zeolites. Otherwise, concerning the discussed material requirements (i.e., enhanced ammonia conversion, N_2 selectivity and stability in the presence of typical components of exhaust gases and the broad temperature range up to 600–700 °C (in the cycle of diesel particulate filter regeneration)), the zeolite-based catalysts present a class of highly promising materials. For instance, ion-exchanged zeolites showed higher activity also in the presence of H_2O, compared to that of alumina-supported oxides with the same metal loading due to high dispersion of metal species and acid sites of high strength. Furthermore, the studies on the reaction mechanisms are rather scarce. The reaction mechanisms must be clarified to rationally develop a process for NH_3 oxidation to N_2 over applied catalysts. These problems highlight the importance of more detailed ex situ and in situ methods (i.e., temperature-programmed, spectroscopic, and/or transient methods) in studying the catalysts under real working environments.

Furthermore, a relatively narrow operating temperature window of full NH_3 conversion (Tables 1–3), high selectivity to N_2O and NO_x, and high costs of noble metals motivated researchers to develop suitable bifunctional systems. Cu-ZSM-5 or even Cu-chabazite (SSZ-13, SAPO-34) are already recognized (also discussed in the previous review articles concerning NH_3-SCO, Jabłońska et al., 2016, Jabłońska et al., 2020) as the active and N_2 selective catalysts for NH_3-SCR. Despite presented here developments in bifunctional catalysts (mainly Pt-Cu or Ag-Cu catalysts systems), challenges remain in achieving enhanced NH_3 conversion, N_2 selectivity, and stability (in the presence of real flue gases, such as H_2O, SO_x, and CO_x). Further investigations concerning bifunctional catalysts with a low number of noble metals, e.g., Au, Pt-Au, Pt-Rh, etc., constitute a promising research direction. Nevertheless, the present findings, indications, and thoughts given in the mini-review form a solid basis for further developments of structured catalysts (i.e., in the form of dual-layer or core-shell structure) and their optimization.

Funding: This research received no external funding.

Acknowledgments: The author acknowledges support from the german Research Foundation (DFG) and Leipzig University within the program of Open Access Publishing.

Conflicts of Interest: The authors declare no conflict of interest.

References

1. Park, S.-J.; Jin, S.-Y. Effect of ozone treatment on ammonia removal of activated carbons. *J. Colloid Interface Sci.* **2005**, *286*, 417–419. [CrossRef]
2. Abe, Y.; Miyata, N.; Yasuda, T. Comparison between direct-dontact HfO_2/Ge and HfO_2/GeO_2/Ge stack structures: Physical and electrical properties. *ECS Trans.* **2008**, *16*, 375. [CrossRef]
3. Karri, R.R.; Sahu, J.N.; Chimmiri, V. Critical review of abatement of ammonia from wastewater. *J. Mol. Liq.* **2018**, *261*, 21–31. [CrossRef]
4. Boardman, G.D.; Starbuck, S.M.; Hudgins, D.B.; Li, X.; Kuhn, D.D. Toxicity of ammonia to three marine fish and three marine invertebrates. *Environ. Toxicol. Int. J.* **2004**, *19*, 134–142. [CrossRef] [PubMed]
5. Camargo, J.A.; Alonso, Á. Ecological and toxicological effects of inorganic nitrogen pollution in aquatic ecosystems: A global assessment. *Environ. Int.* **2006**, *32*, 831–849. [CrossRef] [PubMed]
6. Dammers, E.; McLinden, C.A.; griffin, D.; Shephard, M.W.; graaf, S.V.D.; Lutsch, E.; Schaap, M.; gainairu-Matz, Y.; Fioletov, V.; Damme, M.V.; et al. NH_3 emissions from large point sources derived from CrIS and IASI satellite observations. *Atmos. Chem. Phys.* **2019**, *19*, 12261–12293. [CrossRef]

7. Jabłońska, M.; Palkovits, R. Copper based catalysts for the selective ammonia oxidation into nitrogen and water vapour-Recent trends and open challenges. *Appl. Catal. B Environ.* **2016**, *181*, 332–351. [CrossRef]
8. European Union. Regulation (EC) No 595/2009 of the European Parliament and of the Council of 18 June 2009 on Type-Approval of Motor Vehicles and Engines with Respect to Emissions from Heavy Duty Vehicles (Euro VI) and on Access to Vehicle Repair and Maintenance Informati. *Off. J. Eur. Communities 50* **2009**, *43*, 164–176.
9. Suarez-Bertoa, R.; Mendoza-Villafuerte, P.; Riccobono, F.; Vojtisek, M.; Pechout, M.; Perujo, A.; Astorga, C. On-road measurement of NH_3 emissions from gasoline and diesel passenger cars during real world driving conditions. *Atmos. Environ.* **2017**, *166*, 488–497. [CrossRef]
10. Suarez-Bertoa, R.; Pechout, M.; Vojtíšek, M.; Astorga, C. Regulated and non-regulated emissions from Euro 6 diesel, gasoline and CNG vehicles under real-world driving conditions. *Atmosphere* **2020**, *11*, 204. [CrossRef]
11. Carabineiro, S.A.C.; Matveev, A.V.; gorodetskii, V.V.; Nieuwenhuys, B.E. Selective oxidation of ammonia over Ru (0 0 0 1). *Surf. Sci.* **2004**, *555*, 83–93. [CrossRef]
12. Lin, M.; An, B.; Niimi, N.; Jikihara, Y.; Nakayama, T.; Honma, T.; Takei, T.; Shishido, T.; Ishida, T.; Haruta, M.; et al. Role of the acid site for selective catalytic oxidation of NH_3 over Au/Nb_2O_5. *ACS Catal.* **2019**, *9*, 1753–1756. [CrossRef]
13. Chmielarz, L.; Jabłońska, M.; Strumiński, A.; Piwowarska, Z.; Węgrzyn, A.; Witkowski, S.; Michalik, M. Selective catalytic oxidation of ammonia to nitrogen over Mg-Al, Cu-Mg-Al and Fe-Mg-Al mixed metal oxides doped with noble metals. *Appl. Catal. B Environ.* **2013**, *130*, 152–162. [CrossRef]
14. Chmielarz, L.; Jabłońska, M. Advances in selective catalytic oxidation of ammonia to dinitrogen: A review. *RSC Adv.* **2015**, *5*, 43408–43431. [CrossRef]
15. Gao, F.; Liu, Y.; Sani, Z.; Tang, X.; Yi, H.; Zhao, S.; Yu, Q.; Zhou, Y. Advances in selective catalytic oxidation of ammonia (NH_3-SCO) to dinitrogen in excess oxygen: A review on typical catalysts, catalytic performances and reaction mechanisms. *J. Environ. Chem. Eng.* **2020**, *9*, 104575.
16. Lan, T.; Zhao, Y.; Deng, J.; Zhang, J.; Shi, L.; Zhang, D. Selective catalytic oxidation of NH_3 over noble metal-based catalysts: State of the art and future prospects. *Catal. Sci. Technol.* **2020**, *10*, 5792–5810. [CrossRef]
17. Wang, F.; Ma, J.; He, G.; Chen, M.; Zhang, C.; He, H. Nanosize effect of Al_2O_3 in Ag/Al_2O_3 catalyst for the selective catalytic oxidation of ammonia. *ACS Catal.* **2018**, *8*, 2670–2682. [CrossRef]
18. Li, P.; Zhang, R.; Liu, N.; Royer, S. Efficiency of Cu and Pd substitution in Fe-based perovskites to promote N_2 formation during NH_3 selective catalytic oxidation (NH_3-SCO). *Appl. Catal. B Environ.* **2017**, *203*, 174–188. [CrossRef]
19. Jabłońska, M. Progress on selective catalytic ammonia oxidation (NH_3-SCO) over Cu-containing zeolite-based catalysts. *ChemCatChem* **2020**, *12*, 4490–4500. [CrossRef]
20. Il'chenko, N.I. Catalytic oxidation of ammonia. *Russ. Chem. Rev.* **1976**, *45*, 1119. [CrossRef]
21. Zeng, Y.F.; Imbihl, R. Structure sensitivity of ammonia oxidation over platinum. *J. Catal.* **2009**, *261*, 129–136. [CrossRef]
22. Novell-Leruth, G.; Valcarcel, A.; Pérez-Ramírez, J.; Ricart, J.M. Ammonia dehydrogenation over platinum-group metal surfaces. Structure, stability, and reactivity of adsorbed NH_x species. *J. Phys. Chem. C* **2007**, *111*, 860–868. [CrossRef]
23. Gland, J.L.; Korchak, V.N. Ammonia oxidation on a stepped platinum single-crystal surface. *J. Catal.* **1978**, *53*, 9–23. [CrossRef]
24. Baerns, M.; Imbihl, R.; Kondratenko, V.A.; Kraehnert, R.; Offermans, W.K.; Van Santen, R.A.; Scheibe, A. Bridging the pressure and material gap in the catalytic ammonia oxidation: Structural and catalytic properties of different platinum catalysts. *J. Catal.* **2005**, *232*, 226–238. [CrossRef]
25. Pérez-Ramírez, J.; Kondratenko, E.V.; Novell-Leruth, G.; Ricart, J.M. Mechanism of ammonia oxidation over PGM (Pt, Pd, Rh) wires by temporal analysis of products and density functional theory. *J. Catal.* **2009**, *261*, 217–223. [CrossRef]
26. Ostermaier, J.J.; Katzer, J.R.; Manogue, W.H. Crystallite size effects in the low-temperature oxidation of ammonia over supported platinum. *J. Catal.* **1974**, *33*, 457–473. [CrossRef]
27. Svintsitskiy, D.A.; Slavinskaya, E.M.; Stonkus, O.A.; Romanenko, A.V.; Stadnichenko, A.I.; Kibis, L.S.; Derevyannikova, E.A.; Evtushkova, A.A.; Boronin, A.I. The state of platinum and structural features of Pt/Al_2O_3 catalysts in the reaction of NH_3 oxidation. *J. Struct. Chem.* **2019**, *60*, 919–931. [CrossRef]
28. Bahrami, B.; Komvokis, V.G.; Ziebarth, M.S.; Alexeev, O.S.; Amiridis, M.D. NH_3 decomposition and oxidation over noble metal-based FCC CO combustion promoters. *Appl. Catal. B Environ.* **2013**, *130*, 25–35. [CrossRef]
29. Svintsitskiy, D.A.; Kibis, L.S.; Stadnichenko, A.I.; Slavinskaya, E.M.; Romanenko, A.V.; Fedorova, E.A.; Stonkus, O.A.; Doronkin, D.E.; Marchuk, V.; Zimina, A.; et al. Insight into the nature of active species of Pt/Al_2O_3 catalysts for low temperature NH_3 oxidation. *ChemCatChem* **2020**, *12*, 867–880. [CrossRef]
30. Kibis, L.S.; Svintsitskiy, D.A.; Stadnichenko, A.I.; Slavinskaya, E.M.; Romanenko, A.V.; Fedorova, E.A.; Stonkus, O.A.; Svetlichnyi, V.A.; Fakhrutdinova, E.D.; Vorokhta, M.; et al. In situ probing of Pt/TiO_2 activity in low-temperature ammonia oxidation. *Catal. Sci. Technol.* **2021**, *11*, 250–263. [CrossRef]
31. Liu, J.; Lin, Q.; Liu, S.; Xu, S.; Xu, H.; Chen, Y. Promotional effects of ascorbic acid on the low-temperature catalytic activity of selective catalytic oxidation of ammonia over Pt/SA: Effect of Pt^0 content. *New J. Chem.* **2020**, *44*, 4108–4113. [CrossRef]
32. Ostermaier, J.J.; Katzer, J.R.; Manogue, W.H. Platinum catalyst deactivation in low-temperature ammonia oxidation reactions: I. Oxidation of ammonia by molecular oxygen. *J. Catal.* **1976**, *41*, 277–292. [CrossRef]
33. Sobczyk, D.P.; Van grondelle, J.; Thüne, P.C.; Kieft, I.E.; De Jong, A.M.; Van Santen, R.A. Low-temperature ammonia oxidation on platinum sponge studied with positron emission profiling. *J. Catal.* **2004**, *225*, 466–478. [CrossRef]

34. Sobczyk, D.P.; Hensen, E.J.M.; De Jong, A.M.; Van Santen, R.A. Low-temperature ammonia oxidation over Pt/γ-alumina: The influence of the alumina support. *Top. Catal.* **2003**, *23*, 109–117. [CrossRef]
35. Liu, J.; Sun, M.; Lin, Q.; Liu, S.; Xu, H.; Chen, Y. Promotional effects of ethylenediamine on the low-temperature catalytic activity of selective catalytic oxidation of ammonia over Pt/SiAlO$_x$: States and particle sizes of Pt. *Appl. Surf. Sci.* **2019**, *481*, 1344–1351. [CrossRef]
36. Slavinskaya, E.M.; Kibis, L.S.; Stonkus, O.A.; Svintsitskiy, D.A.; Stadnichenko, A.I.; Fedorova, E.A.; Romanenko, A.V.; Marchuk, V.; Doronkin, D.E.; Boronin, A.I. The effects of platinum dispersion and Pt state on catalytic properties of Pt/Al_2O_3 in NH_3 oxidation. *ChemCatChem* **2020**, *13*, 313–327. [CrossRef]
37. Dhillon, P.S.; Harold, M.P.; Wang, D.; Kumar, A.; Joshi, S. Hydrothermal aging of Pt/Al_2O_3 monolith: Washcoat morphology degradation effects studied using ammonia and propylene oxidation. *Catal. Today* **2019**, *320*, 20–29. [CrossRef]
38. Machida, M.; Tokudome, Y.; Maeda, A.; Kuzuhara, Y.; Hirakawa, T.; Sato, T.; Yoshida, H.; Ohyama, J.; Fujii, K.; Ishikawa, N. Nanometric platinum overlayer to catalyze NH_3 oxidation with high turnover frequency. *ACS Catal.* **2020**, *10*, 4677–4685. [CrossRef]
39. Mieher, W.D.; Ho, W. Thermally activated oxidation of NHs on Pt (111): Intermediate species and reaction mechanisms. *Surf. Sci.* **1995**, *322*, 151–167. [CrossRef]
40. Offermans, W.K.; Jansen, A.P.J.; Van Santen, R.A. Ammonia activation on platinum {111}: A density functional theory study. *Surf. Sci.* **2006**, *600*, 1714–1734. [CrossRef]
41. Novell-Leruth, G.; Ricart, J.M.; Pérez-Ramírez, J. Pt (100)-catalyzed ammonia oxidation studied by DFT: Mechanism and microkinetics. *J. Phys. Chem. C* **2008**, *112*, 13554–13562. [CrossRef]
42. Sun, M.; Liu, J.; Song, C.; Ogata, Y.; Rao, H.; Zhao, X.; Xu, H.; Chen, Y. Different reaction mechanisms of ammonia oxidation reaction on Pt/Al_2O_3 and Pt/$CeZrO_2$ with various Pt states. *ACS Appl. Mater. Interfaces* **2019**, *11*, 23102–23111. [CrossRef] [PubMed]
43. Li, Y.; Armor, J.N. Selective NH_3 oxidation to N_2 in a wet stream. *Appl. Catal. B Environ.* **1997**, *13*, 131–139. [CrossRef]
44. Long, R.Q.; Yang, R.T. Superior ion-exchanged ZSM-5 catalysts for selective catalytic oxidation of ammonia to nitrogen. *Chem. Commun.* **2000**, *17*, 1651–1652. [CrossRef]
45. Jabłońska, M.; Król, A.; Kukulska-Zając, E.; Tarach, K.; Chmielarz, L.; Góra-Marek, K. Zeolite Y modified with palladium as effective catalyst for selective catalytic oxidation of ammonia to nitrogen. *J. Catal.* **2014**, *316*, 36–46. [CrossRef]
46. Decarolis, D.; Clark, A.H.; Pellegrinelli, T.; Nachtegaal, M.; Lynch, E.W.; Catlow, C.R.A.; gibson, E.K.; goguet, A.; Wells, P.P. Spatial profiling of a Pd/Al_2O_3 Cctalyst during selective ammonia oxidation. *ACS Catal.* **2021**, *11*, 2141–2149. [CrossRef]
47. Dann, E.K.; gibson, E.K.; Blackmore, R.H.; Catlow, C.R.A.; Collier, P.; Chutia, A.; Erden, T.E.; Hardacre, C.; Kroner, A.; Nachtegaal, M.; et al. Structural selectivity of supported Pd nanoparticles for catalytic NH_3 oxidation resolved using combined operando spectroscopy. *Nat. Catal.* **2019**, *2*, 157–163. [CrossRef]
48. Jabłońska, M. TPR study and catalytic performance of noble metals modified Al_2O_3, TiO_2 and ZrO_2 for low-temperature NH_3-SCO. *Catal. Commun.* **2015**, *70*, 66–71. [CrossRef]
49. Olofsson, G.; Wallenberg, L.R.; Andersson, A. Selective catalytic oxidation of ammonia to nitrogen at low temperature on Pt/CuO/Al_2O_3. *J. Catal.* **2005**, *230*, 1–13. [CrossRef]
50. Burch, R.; Southward, B.W.L. Low-temperature, clean catalytic combustion of N-bearing gasified biomass using a novel NH_3 trapping catalyst. *Chem. Commun.* **2000**, *13*, 1115–1116. [CrossRef]
51. Kušar, H.M.J.; Ersson, A.G.; Vosecký, M.; Järås, S.G. Selective catalytic oxidation of NH_3 to N_2 for catalytic combustion of low heating value gas under lean/rich conditions. *Appl. Catal. B Environ.* **2005**, *58*, 25–32. [CrossRef]
52. Burch, R.; Southward, B.W.L. A novel application of trapping catalysts for the selective low-temperature oxidation of NH_3 to N_2 in simulated biogas. *J. Catal.* **2000**, *195*, 217–226. [CrossRef]
53. Sun, M.; Wang, S.; Li, Y.; Xu, H.; Chen, Y. Promotion of catalytic performance by adding W into Pt/ZrO_2 catalyst for selective catalytic oxidation of ammonia. *Appl. Surf. Sci.* **2017**, *402*, 323–329. [CrossRef]
54. Long, R.Q.; Yang, R.T. Noble metal (Pt, Rh, Pd) promoted Fe-ZSM-5 for selective catalytic oxidation of ammonia to N_2 at low temperatures. *Catal. Lett.* **2002**, *78*, 353–357. [CrossRef]
55. Kim, M.-S.; Lee, D.-W.; Chung, S.-H.; Hong, Y.-K.; Lee, S.H.; Oh, S.-H.; Cho, I.-H.; Lee, K.-Y. Oxidation of ammonia to nitrogen over Pt/Fe/ZSM5 catalyst: Influence of catalyst support on the low temperature activity. *J. Hazard. Mater.* **2012**, *237*, 153–160. [CrossRef]
56. Abbas-Ghaleb, R.; Chlala, D. Selective catalytic oxidation of NH_3 into N_2 during biogas combustion over 2 wt% PdO/5 wt% CuO/γ-Al_2O_3. *SN Appl. Sci.* **2020**, *2*, 592–599. [CrossRef]
57. Shrestha, S.; Harold, M.P.; Kamasamudram, K.; Yezerets, A. Ammonia oxidation on structured composite catalysts. *Top. Catal.* **2013**, *56*, 182–186. [CrossRef]
58. Shrestha, S.; Harold, M.P.; Kamasamudram, K.; Yezerets, A. Selective oxidation of ammonia on mixed and dual-layer Fe-ZSM-5+Pt/Al_2O_3 monolithic catalysts. *Catal. Today* **2014**, *231*, 105–115. [CrossRef]
59. Shrestha, S.; Harold, M.P.; Kamasamudram, K.; Kumar, A.; Olsson, L.; Leistner, K. Selective oxidation of ammonia to nitrogen on bi-functional Cu-SSZ-13 and Pt/Al_2O_3 monolith catalyst. *Catal. Today* **2016**, *267*, 130–144. [CrossRef]
60. Scheuer, A.; Hauptmann, W.; Drochner, A.; gieshoff, J.; Vogel, H.; Votsmeier, M. Dual layer automotive ammonia oxidation catalysts: Experiments and computer simulation. *Appl. Catal. B Environ.* **2012**, *111*, 445–455. [CrossRef]

61. Colombo, M.; Nova, I.; Tronconi, E.; Schmeißer, V.; Bandl-Konrad, B.; Zimmermann, L. Experimental and modeling study of a dual-layer (SCR+ PGM) NH_3 slip monolith catalyst (ASC) for automotive SCR aftertreatment systems. Part 1. Kinetics for the PGM component and analysis of SCR/PGM interactions. *Appl. Catal. B Environ.* **2013**, *142*, 861–876. [CrossRef]
62. Dhillon, P.S.; Harold, M.P.; Wang, D.; Kumar, A.; Joshi, S.Y. Enhanced transport in washcoated monoliths: Application to selective lean NO_x reduction and ammonia oxidation. *Chem. Eng. J.* **2019**, *377*, 119734. [CrossRef]
63. Ghosh, R.S.; Le, T.T.; Terlier, T.; Rimer, J.D.; Harold, M.P.; Wang, D. Enhanced selective oxidation of ammonia in a Pt/Al_2O_3@ Cu/ZSM-5 core-shell catalyst. *ACS Catal.* **2020**, *10*, 3604–3617. [CrossRef]
64. Dhillon, P.S.; Harold, M.P.; Wang, D.; Kumar, A.; Joshi, S.Y. Optimizing the dual-layer Pt/Al_2O_3+Cu/SSZ-13 washcoated monolith: Selective oxidation of NH_3 to N_2. *Catal. Today* **2021**, *360*, 426–434. [CrossRef]
65. Hung, C.-M.; Lai, W.-L.; Lin, J.-L. Removal of gaseous ammonia in Pt-Rh binary catalytic oxidation. *Aerosol Air Qual. Res.* **2012**, *12*, 583–591. [CrossRef]
66. Hung, C.-M. Fabrication, characterization, and evaluation of the cytotoxicity of platinum-rhodium nanocomposite materials for use in ammonia treatment. *Powder Technol.* **2011**, *209*, 29–34. [CrossRef]
67. Gang, L.; Anderson, B.G.; Van grondelle, J.; Van Santen, R.A. NH_3 oxidation to nitrogen and water at low temperatures using supported transition metal catalysts. *Catal. Today* **2000**, *61*, 179–185. [CrossRef]
68. Chang, S.; Harle, G.; Ma, J.; Yi, J. The effect of textural Properties of CeO_2-SiO_2 mixed oxides on NH_3-SCO activity of Pt/CeO_2-SiO_2 catalyst. *Appl. Catal. A gen.* **2020**, *604*, 117775. [CrossRef]
69. Kim, G.J.; Kwon, D.W.; Shin, J.H.; Kim, K.W.; Hong, S.C. Influence of the addition of vanadium to Pt/TiO_2 catalyst on the selective catalytic oxidation of NH_3 to N_2. *Environ. Technol.* **2019**, *40*, 2588–2600. [CrossRef] [PubMed]
70. Il'chenko, N.I.; golodets, G.I.; Avilova, I.M. Oxidation of ammonia on metals. [Catalytic activity of Pt, Pd, Cu, Ag, Ni, Au, Fe, W, and Ti]. *Kinet. Catal. (USSR) (Engl. Transl.) (USA)* **1975**, *16*, 1455–1460.
71. Gang, L.; Anderson, B.G.; Van grondelle, J.; Van Santen, R.A.; Van gennip, W.J.H.; Niemantsverdriet, J.W.; Kooyman, P.J.; Knoester, A.; Brongersma, H.H. Alumina-supported Cu-Ag catalysts for ammonia oxidation to nitrogen at low temperature. *J. Catal.* **2002**, *206*, 60–70. [CrossRef]
72. Gang, L.; Anderson, B.G.; Van grondelle, J.; Van Santen, R.A. Low temperature selective oxidation of ammonia to nitrogen on silver-based catalysts. *Appl. Catal. B Environ.* **2003**, *40*, 101–110. [CrossRef]
73. Zhang, L.; He, H. Mechanism of selective catalytic oxidation of ammonia to nitrogen over Ag/Al_2O_3. *J. Catal.* **2009**, *268*, 18–25. [CrossRef]
74. Zhang, L.; Zhang, C.; He, H. The role of silver species on Ag/Al_2O_3 catalysts for the selective catalytic oxidation of ammonia to nitrogen. *J. Catal.* **2009**, *261*, 101–109. [CrossRef]
75. Zhang, L.; Fudong, L.I.U.; Yunbo, Y.U.; Yongchun, L.I.U.; Zhang, C.; Hong, H.E. Effects of adding CeO_2 to Ag/Al_2O_3 catalyst for ammonia oxidation at low temperatures. *Chin. J. Catal.* **2011**, *32*, 727–735. [CrossRef]
76. Wang, F.; He, G.; Zhang, B.; Chen, M.; Chen, X.; Zhang, C.; He, H. Insights into the activation effect of H_2 pretreatment on Ag/Al_2O_3 catalyst for the selective oxidation of ammonia. *ACS Catal.* **2019**, *9*, 1437–1445. [CrossRef]
77. Lippits, M.J.; gluhoi, A.C.; Nieuwenhuys, B.E. A comparative study of the selective oxidation of NH_3 to N_2 over gold, silver and copper catalysts and the effect of addition of Li_2O and CeO_x. *Catal. Today* **2008**, *137*, 446–452. [CrossRef]
78. Qu, Z.; Wang, H.; Wang, S.; Cheng, H.; Qin, Y.; Wang, Z. Role of the support on the behavior of Ag-based catalysts for NH_3 selective catalytic oxidation (NH_3-SCO). *Appl. Surf. Sci.* **2014**, *316*, 373–379. [CrossRef]
79. Yang, M.; Wu, C.; Zhang, C.; He, H. Selective oxidation of ammonia over copper-silver-based catalysts. *Catal. Today* **2004**, *90*, 263–267. [CrossRef]
80. Jabłońska, M.; Beale, A.M.; Nocuń, M.; Palkovits, R. Ag-Cu based catalysts for the selective ammonia oxidation into nitrogen and water vapour. *Appl. Catal. B Environ.* **2018**, *232*, 275–287. [CrossRef]
81. Wang, F.; Ma, J.; He, G.; Chen, M.; Wang, S.; Zhang, C.; He, H. Synergistic effect of TiO_2-SiO_2 in Ag/Si-Ti catalyst for the selective catalytic oxidation of ammonia. *Ind. Eng. Chem. Res.* **2018**, *57*, 11903–11910. [CrossRef]
82. Jabłońska, M.; Ciptonugroho, W.; Góra-Marek, K.; Al-Shaal, M.G.; Palkovits, R. Preparation, characterization and catalytic performance of Ag-modified mesoporous TiO_2 in low-temperature selective ammonia oxidation into nitrogen and water vapour. *Microporous Mesoporous Mater.* **2017**, *245*, 31–44. [CrossRef]
83. Wang, Z.; Sun, Q.; Wang, D.; Hong, Z.; Qu, Z.; Li, X. Hollow ZSM-5 zeolite encapsulated Ag nanoparticles for SO_2-resistant selective catalytic oxidation of ammonia to nitrogen. *Sep. Purif. Technol.* **2019**, *209*, 1016–1026. [CrossRef]
84. Gang, L.; Anderson, B.G.; Van grondelle, J.; Van Santen, R.A. Intermediate species and reaction pathways for the oxidation of ammonia on powdered catalysts. *J. Catal.* **2001**, *199*, 107–114. [CrossRef]
85. Karatok, M.; Vovk, E.I.; Koc, A.V.; Ozensoy, E. Selective catalytic ammonia oxidation to nitrogen by atomic oxygen species on Ag (111). *J. Phys. Chem. C* **2017**, *121*, 22985–22994. [CrossRef]
86. Carabineiro, S.A.C.; Nieuwenhuys, B.E. Selective oxidation of ammonia over Ir (510). Comparison with Ir (110). *Surf. Sci.* **2003**, *532*, 87–95. [CrossRef]
87. Jabłońska, M.; Nothdurft, K.; Nocuń, M.; girman, V.; Palkovits, R. Redox-performance correlations in Ag–Cu–Mg–Al, Ce–Cu–Mg–Al, and ga–Cu–Mg–Al hydrotalcite derived mixed metal oxides. *Appl. Catal. B Environ.* **2017**, *207*, 385–396. [CrossRef]
88. Qu, Z.; Wang, Z.; Quan, X.; Wang, H.; Shu, Y. Selective catalytic oxidation of ammonia to N_2 over wire-mesh honeycomb catalyst in simulated synthetic ammonia stream. *Chem. Eng. J.* **2013**, *233*, 233–241. [CrossRef]

89. Zhou, M.; Wang, Z.; Sun, Q.; Wang, J.; Zhang, C.; Chen, D.; Li, X. High-performance Ag-Cu nanoalloy catalyst for the selective catalytic oxidation of ammonia. *ACS Appl. Mater. Interfaces* **2019**, *11*, 46875–46885. [CrossRef] [PubMed]
90. Wang, H.; Lin, M.; Murayama, T.; Feng, S.; Haruta, M.; Miura, H.; Shishido, T. Ag size/structure-dependent effect on low-temperature selective catalytic oxidation of NH_3 over Ag/MnO_2. *ACS Catal.* **2021**, *11*, 8576–8584. [CrossRef]
91. Góra-Marek, K.; Tarach, K.A.; Piwowarska, Z.; Łaniecki, M.; Chmielarz, L. Ag-loaded zeolites Y and USY as catalysts for selective ammonia oxidation. *Catal. Sci. Technol.* **2016**, *6*, 1651–1660. [CrossRef]
92. Martinez-Ortigosa, J.; Lopes, C.W.; Agostini, G.; Palomares, A.E.; Blasco, T.; Rey, F. AgY zeolite as catalyst for the selective catalytic oxidation of NH_3. *Microporous Mesoporous Mater.* **2021**, *323*, 111230. [CrossRef]
93. Guzman, J.; gates, B.C. Catalysis by supported gold: Correlation between catalytic activity for CO oxidation and oxidation states of gold. *J. Am. Chem. Soc.* **2004**, *126*, 2672–2673. [CrossRef] [PubMed]
94. Kaskow, I.; Sobczak, I.; Ziolek, M.; Corberán, V.C. The effect of support properties on n-octanol oxidation performed on gold-silver catalysts supported on MgO, ZnO and Nb_2O_5. *Mol. Catal.* **2020**, *482*, 110674. [CrossRef]
95. Lin, S.D.; gluhoi, A.C.; Nieuwenhuys, B.E. Ammonia oxidation over $Au/MO_x/\gamma\text{-}Al_2O_3$—Activity, selectivity and FTIR measurements. *Catal. Today* **2004**, *90*, 3–14. [CrossRef]
96. Gong, J.; Ojifinni, R.A.; Kim, T.S.; White, J.M.; Mullins, C.B. Selective catalytic oxidation of ammonia to nitrogen on atomic oxygen precovered Au (111). *J. Am. Chem. Soc.* **2006**, *128*, 9012–9013. [CrossRef]
97. Liu, R.; Shen, W.; Zhang, J.; Li, M. Adsorption and dissociation of ammonia on Au (111) surface: A density functional theory study. *Appl. Surf. Sci.* **2008**, *254*, 5706–5710. [CrossRef]
98. Wang, Y.; Jacobi, K.; Schöne, W.-D.; Ertl, G. Catalytic oxidation of ammonia on RuO_2 (110) surfaces: Mechanism and selectivity. *J. Phys. Chem. B* **2005**, *109*, 7883–7893. [CrossRef]
99. Seitsonen, A.P.; Crihan, D.; Knapp, M.; Resta, A.; Lundgren, E.; Andersen, J.N.; Over, H. Reaction mechanism of ammonia oxidation over RuO2 (110): A combined theory/experiment approach. *Surf. Sci.* **2009**, *603*, L113–L116. [CrossRef]
100. Perez-Ramirez, J.; López, N.; Kondratenko, E.V. Pressure and materials effects on the selectivity of RuO_2 in NH_3 oxidation. *J. Phys. Chem. C* **2010**, *114*, 16660–16668. [CrossRef]
101. Cui, X.; Chen, L.; Wang, Y.; Chen, H.; Zhao, W.; Li, Y.; Shi, J. Fabrication of hierarchically porous RuO_2-CuO/Al-ZrO_2 composite as highly efficient catalyst for ammonia-selective catalytic oxidation. *ACS Catal.* **2014**, *4*, 2195–2206. [CrossRef]
102. Cui, X.; Zhou, J.; Ye, Z.; Chen, H.; Li, L.; Ruan, M.; Shi, J. Selective catalytic oxidation of ammonia to nitrogen over mesoporous CuO/RuO_2 synthesized by co-nanocasting-replication method. *J. Catal.* **2010**, *270*, 310–317. [CrossRef]
103. Chakraborty, D.; Damsgaard, C.D.; Silva, H.; Conradsen, C.; Olsen, J.L.; Carvalho, H.W.P.; Mutz, B.; Bligaard, T.; Hoffmann, M.J.; grunwaldt, J.-D.; et al. Bottom-up design of a copper-ruthenium nanoparticulate catalyst for low-temperature ammonia oxidation. *Angew. Chem.* **2017**, *129*, 8837–8841. [CrossRef]
104. Wang, H.; Ning, P.; Zhang, Q.; Liu, X.; Zhang, T.; Fan, J.; Wang, J.; Long, K. Promotional mechanism of WO_3 over RuO_2-Fe_2O_3 catalyst for NH_3-SCO reaction. *Appl. Catal. A gen.* **2018**, *561*, 158–167. [CrossRef]
105. Chen, W.; Ma, Y.; Qu, Z.; Liu, Q.; Huang, W.; Hu, X.; Yan, N. Mechanism of the selective catalytic oxidation of slip ammonia over Ru-modified Ce-Zr complexes determined by in situ diffuse reflectance infrared Fourier transform spectroscopy. *Environ. Sci. Technol.* **2014**, *48*, 12199–12205. [CrossRef]
106. Chen, W.; Qu, Z.; Huang, W.; Hu, X.; Yan, N. Novel effect of SO_2 on selective catalytic oxidation of slip ammonia from coal-fired flue gas over IrO_2 modified Ce-Zr solid solution and the mechanism investigation. *Fuel* **2016**, *166*, 179–187. [CrossRef]
107. Zhang, Q.; Zhang, T.; Xia, F.; Zhang, Y.; Wang, H.; Ning, P. Promoting effects of acid enhancing on N_2 selectivity for selectivity catalytic oxidation of NH_3 over RuO_x/TiO_2: The mechanism study. *Appl. Surf. Sci.* **2020**, *500*, 144044. [CrossRef]
108. Liao, Y.; Xu, H.; Li, Z.; Ji, L.; Wang, L.; Gao, G.; Huang, W.; Qu, Z.; Yan, N. Boosting RuO_2 surface reactivity by Cu active sites over Ru/Cu-SSZ-13 for simultaneous catalytic oxidation of CO and NH_3. *J. Phys. Chem. C* **2021**, *125*, 17031–17041. [CrossRef]
109. Heylen, S.; Delcour, N.; Kirschhock, C.E.A.; Martens, J.A. Selective catalytic oxidation of ammonia into dinitrogen over a zeolite-supported ruthenium dioxide catalyst. *ChemCatChem* **2012**, *4*, 1162–1166. [CrossRef]
110. Shin, J.H.; Kim, G.J.; Hong, S.C. Reaction properties of ruthenium over Ru/TiO_2 for selective catalytic oxidation of ammonia to nitrogen. *Appl. Surf. Sci.* **2020**, *506*, 144906. [CrossRef]